GULF GENERAL ATOMIC

Gulf-GA-A12515

HTGR BASE PROGRAM

QUARTERLY PROGRESS REPORT

FOR THE PERIOD ENDING

FEBRUARY 28, 1973

Prepared under
Contract AT(04-3)-167
Project Agreement No. 17
for the
San Francisco Operations Office
U.S. Atomic Energy Commission

Gulf General Atomic Project 317

Date Published - March 30, 1973

GULF GENERAL ATOMIC COMPANY
P.O. BOX 81608, SAN DIEGO, CALIFORNIA 92138

QUARTERLY REPORT SERIES

GA-4072-December, 1962, through February, 1963
GA-4350-March, 1963, through May, 1963
GA-4569-June, 1963, through August, 1963
GA-4937-September, 1963, through November, 1963
GA-5104-December, 1963, through February, 1964
GA-5366-March, 1964, through May, 1964
GA-5618-June, 1964, through August, 1964
GA-5866-September, 1964, through November, 1964
GA-6113-December, 1964, through February, 1965
GA-6418-March, 1965, through May, 1965
GA-6671-June, 1965, through August, 1965
GA-6869-September, 1965, through November, 1965
GA-7010-December, 1965, through February, 1966
GA-7181-March, 1966, through May, 1966
GA-7396-June, 1966, through August, 1966
GA-7553-September, 1966, through November, 1966
GA-7801-December, 1966, through February, 1967
GA-7981-March, 1967, through May, 1967
GA-8200-June, 1967, through August, 1967
GA-8356-September, 1967, through November, 1967
GA-8530-December, 1967, through February, 1968
GA-8662-March, 1968, through May, 1968
GA-8860-June, 1968, through August, 1968
GA-9090-September, 1968, through November, 1968
GA-9227-December, 1968, through February, 1969
GA-9372-March, 1969, through May, 1969
GA-9660-June, 1969, through August, 1969
GA-9815-September, 1969, through November, 1969
GA-9944-December, 1969, through February, 1970
GA-10088-March, 1970, through May, 1970
GA-10288-June, 1970, through August, 1970
GA-10399-September, 1970, through November, 1970
GA-10501-December, 1970, through February, 1971
GA-10661-March, 1971, through May, 1971
Gulf-GA-A10784-June, 1971, through August, 1971
Gulf-GA-A10930-September, 1971, through November, 1971
Gulf-GA-A10999-December, 1971, through February, 1972
Gulf-GA-A12150-March, 1972, through May, 1972
Gulf-GA-A12222-June, 1972, through August, 1972
Gulf-GA-A12422-September, 1972, through November, 1972

ABSTRACT

This publication continues the quarterly report series on the HTGR Base Program. The Program covers items of the base technology of the High-Temperature Gas-cooled Reactor (HTGR) system. The development of the HTGR system will, in part, meet the greater national objective of more effective and efficient utilization of our national resources. The work reported here includes studies of basic fission-product distribution mechanisms, recycle fuel studies (including designing and testing of recycle test elements) and exploration of head-end reprocessing methods (as part of a national recycle plan and of a recycle fuel plan), and physics and fuel management studies. Materials studies include irradiation and analysis of fuel particles in capsules to evaluate fuel systems, and basic studies of control materials and of carbon and graphite. Experimental procedures and results are discussed and, where appropriate, the data are presented in tables, graphs, and photographs. More detailed descriptions of experimental work are presented in topical reports, and these are listed at the end of the report for those concerned with the field.

INTRODUCTION

This report covers the work performed by Gulf General Atomic under U.S. Atomic Energy Commission Contract AT(04-3)-167, Project Agreement No. 17. This Project Agreement calls for support of basic technology associated with gas-cooled, nuclear power reactor systems. The program is based on the concept of the High-temperature Gas-cooled Reactor (HTGR) developed by Gulf General Atomic.

Large HTGR systems will be placed in operation starting in the late 1970's following the operation of the 330-MW(e) prototype in 1973. Characteristics of these advanced systems include:

1. A single-phase gas coolant allowing generation of high-temperature, high-pressure steam with consequent high-efficiency energy conversion and low thermal discharge.

2. A prestressed concrete reactor vessel (PCRV) offering advantages in field construction, primary system integrity, and stressed member inspectability.

3. Graphite core material assuring high-temperature structural strength, large temperature safety margins, and good neutron economy.

4. Thorium fuel cycle leading to U-233 fuel which allows good utilization of nuclear resources and minimum demands on separative work.

CONTENTS

FIGURES

TABLES

TASK IV

FISSION PRODUCT MECHANISMS

FIPER CODE ANALYSIS OF PEACH BOTTOM D13-05 FUEL ELEMENT ACTIVITY PROFILES

Analyses, using the FIPER Q version of the FIPER code (Ref. 4.1), were made of the Sr-89, Sr-90, Cs-134, and Cs-137 fission product activity (concentration) profiles of radial sections taken from the spine and sleeve graphite of Peach Bottom fuel element D13-05. This fuel element was one of 804 fuel elements in Core 1 of the Peach Bottom HTGR. Core 1 operated for 452 effective full power days before shutdown (October 1969). Fuel element D13-05 was returned to Gulf General Atomic for postirradiation examination.

An analysis of the sleeve concentration profiles is given in the present report. Results of an analysis of the spine concentration profiles were reported in the previous Quarterly Progress Report (Gulf-GA-A12422). Included in the previous report were (1) a description of the fuel element, (2) sample positions, (3) sampling procedure and analysis, and (4) temperature profiles.

Summary

As reported in the previous Quarterly Progress Report (Gulf-GA-A12422), the Cs-134 and Cs-137 profiles for the spine appear to be due to both cesium metal diffusion and gaseous precursor diffusion. The profiles are fitted quite closely by curves calculated using the FIPER code. Analysis of the cesium metal diffusion profiles, obtained by subtracting out the gaseous precursor profiles, yielded diffusion coefficient data for cesium in graphite. The data show a value of 7×10^{-9} cm^2/sec at 1000°C and an activation energy of 27 kcal/mole. The Sr-89 and Sr-90 activity profiles for the spine appear to have resulted from the decay of their gaseous precursors Kr-89 and Kr-90. Thus, the strontium data yielded only information on the diffusion of the precursors.

As described in the present report, the Cs-137 and Cs-134 concentration profiles for the sleeve graphite were analyzed using (1) the FIPER code and (2) an equation taking account of backflow of helium through the sleeve graphite. It was concluded that no section of the sleeve concentration profiles can be shown to be due solely to the metal component or gaseous component, as was the case for the spine data. Therefore, no cesium metal diffusion coefficients were obtained for the sleeve graphite.

The Sr-89 and Sr-90 concentration profiles for the sleeve appear to have resulted from the decay of their gaseous precursors Kr-89 and Kr-90. Thus, the strontium data yielded only information on the diffusion of the precursors and no strontium metal diffusion data were obtained.

Procedure

Samples of spine and sleeve graphite were taken from seven different positions along the length of the fuel element. The graphite samples were sectioned by turning the samples on a lathe and uniformly removing a layer of graphite for each section. Weighed samples of the sections were analyzed using gamma-counting and radiochemical techniques.

Analysis of Cesium Concentration Profiles for the Sleeve Graphite

Cesium concentration profile data were obtained for four sleeve positions. The data are plotted in Figs. 4.1 through 4.4. Comparison of the temperatures for the spine and sleeve given in Tables 4.3 and 4.4 in the previous Quarterly Progress Report (Gulf-GA-A12422) shows that the range of temperatures in sleeve positions 2, 5, and 9 is very similar to the temperatures of spine positions 2 and 5. The concentration profiles for the spines in these two positions are made up almost entirely by the precursor component. Therefore, it is expected that the concentration profiles in sleeve positions 2, 5, and 9 will also be made up almost entirely by the precursor component. The temperature in sleeve position 29 is similar to

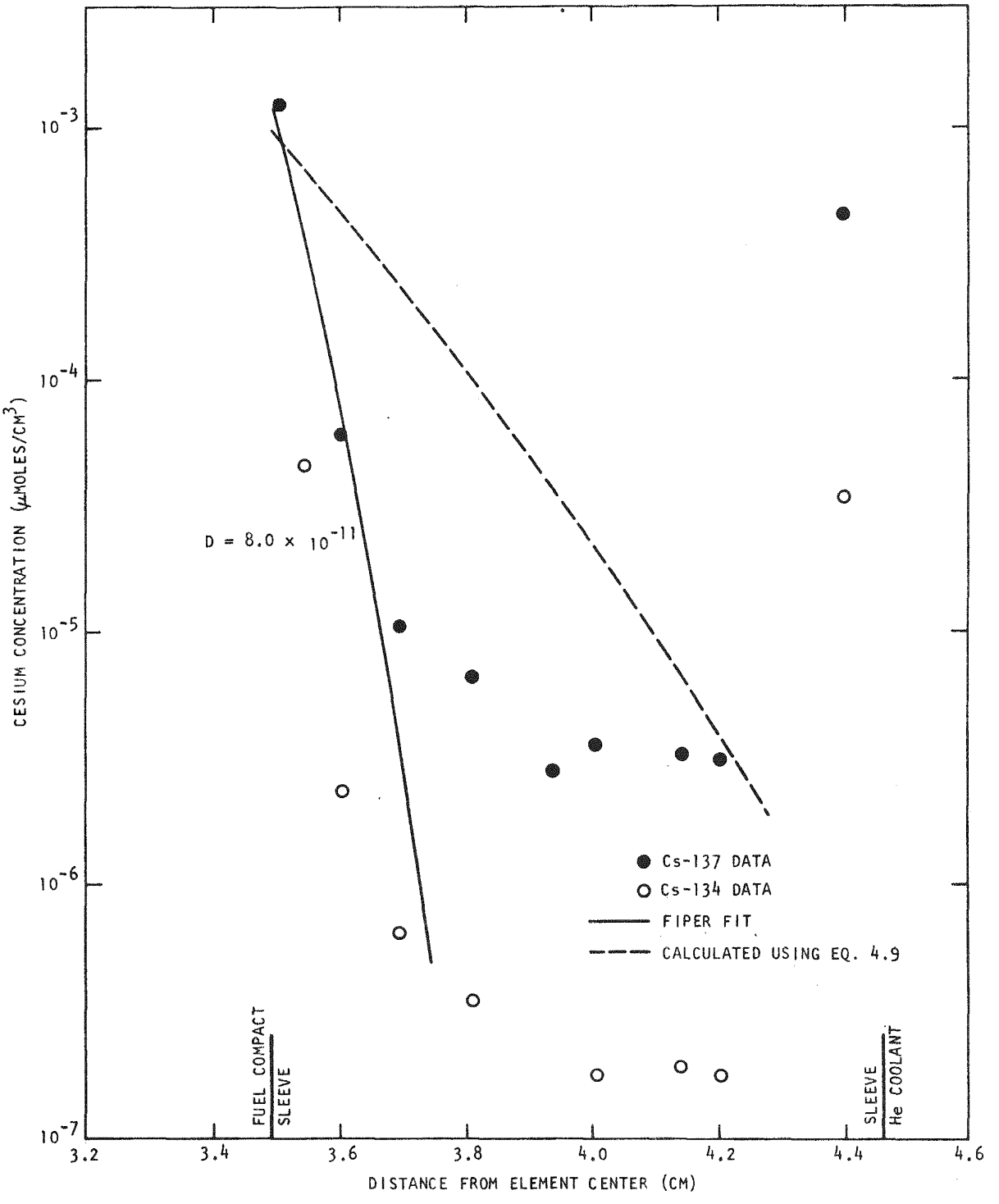

Fig. 4.1. Comparison of measured cesium concentration profile data and calculated profiles for Peach Bottom Core 1, D13-05 fuel element, sleeve position 2

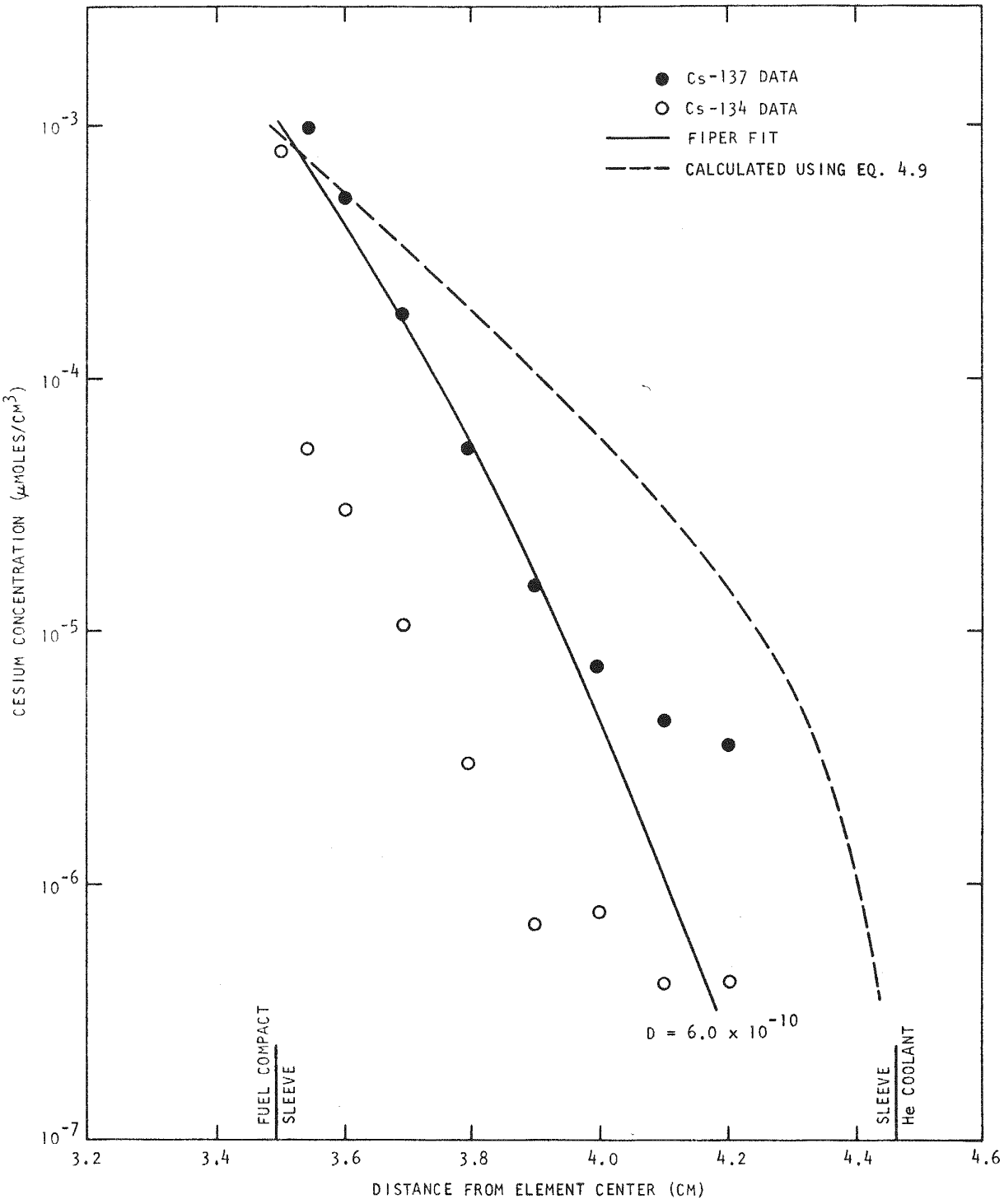

Fig. 4.2. Comparison of measured cesium concentration profile data and calculated profiles for Peach Bottom Core 1, D13-05 fuel element, sleeve position 5

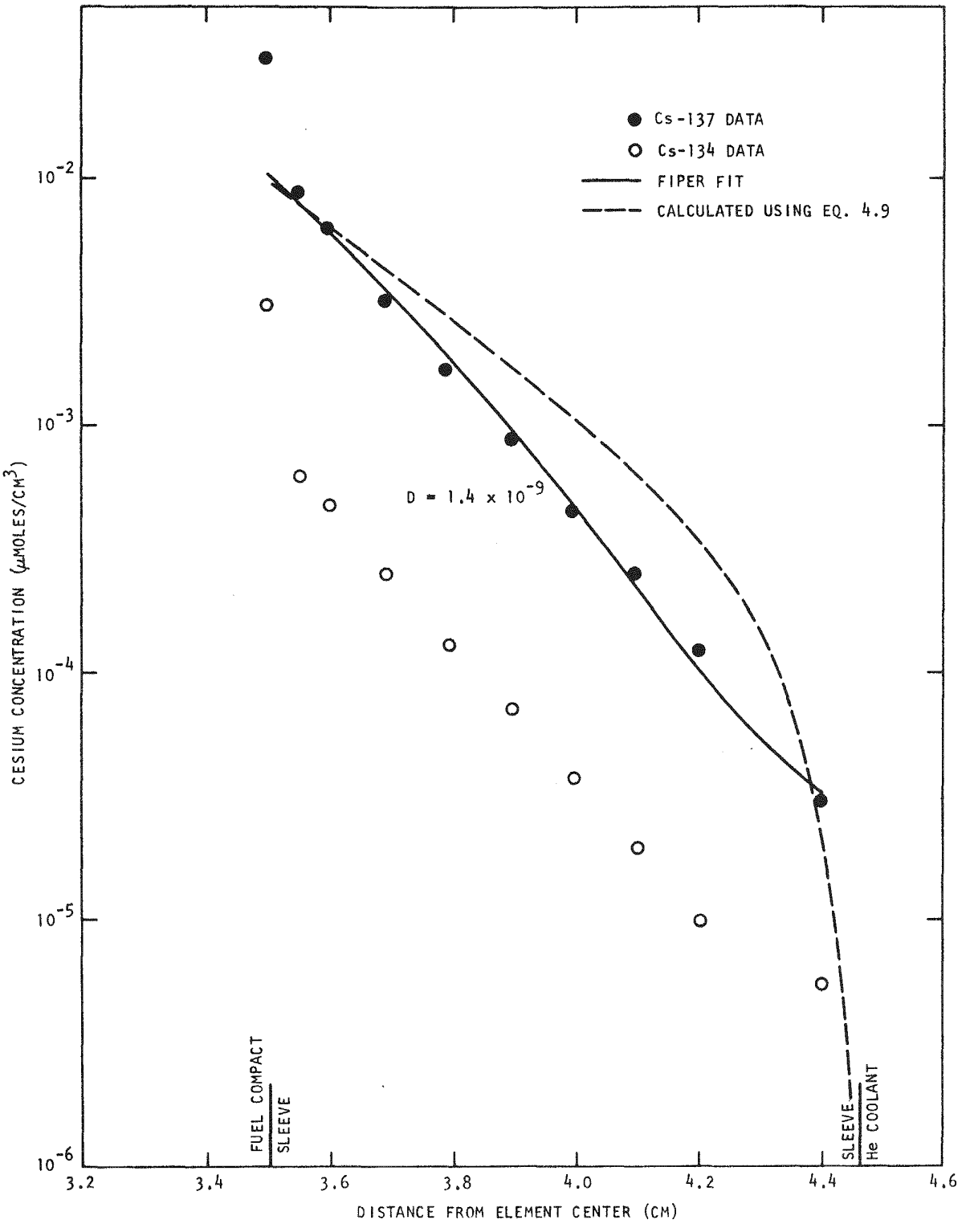

Fig. 4.3. Comparison of measured cesium concentration profile data and calculated profiles for Peach Bottom Core 1, D13-05 fuel element, sleeve position 9

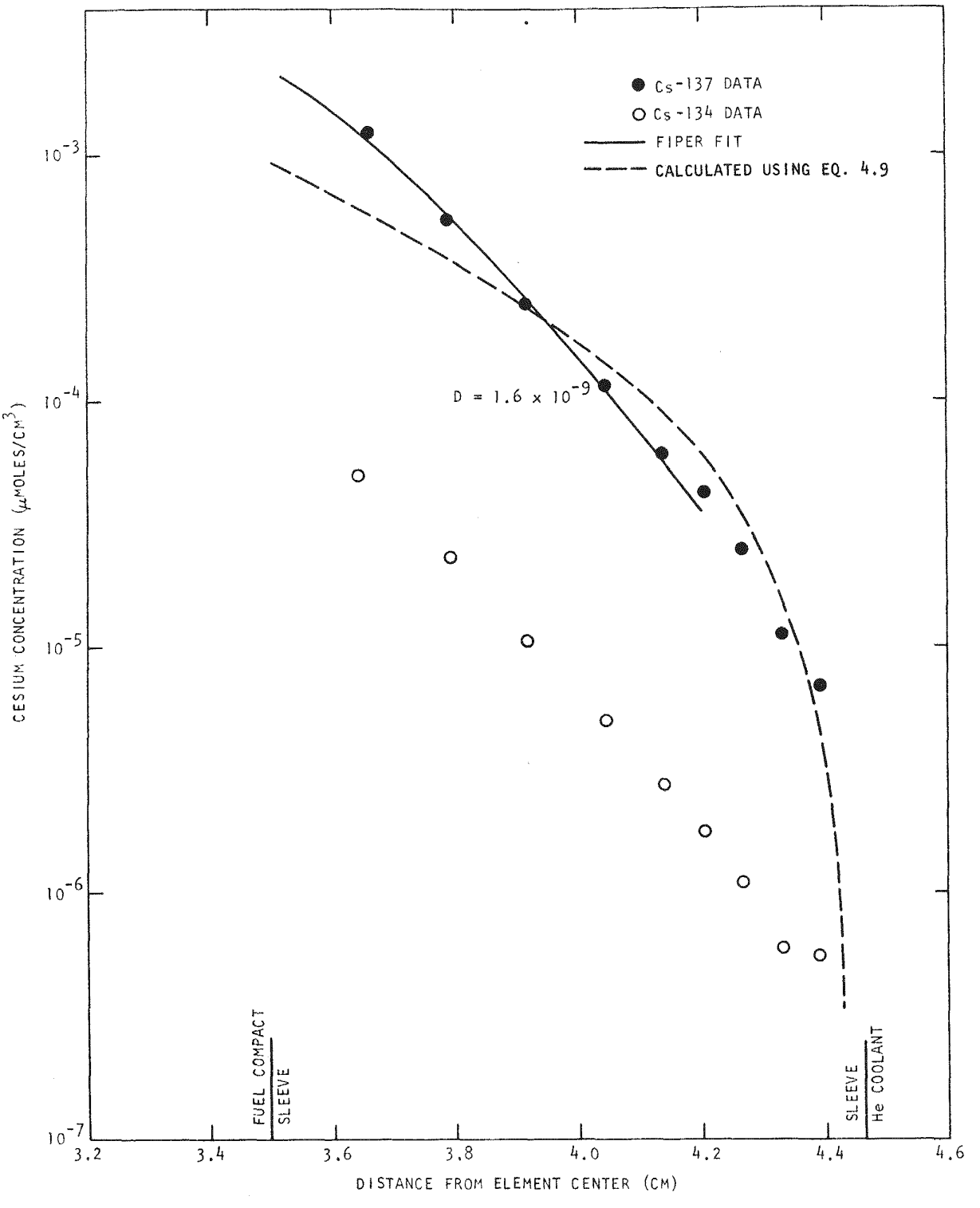

Fig. 4.4. Comparison of measured cesium concentration profile data and calculated profiles for Peach Bottom Core 1, D13-05 fuel element, sleeve position 29

the temperature in spine position 9. The precursor contribution to spine position 9 also makes a significant contribution to the profile. Thus, because of the relative low temperatures of the sleeves, the precursor component might be expected to dominate the metal profile component.

Another factor to be considered is a pressure difference between the helium coolant channel and purge grooves, which causes helium to flow from the coolant through the sleeve into the purge stream. Therefore, the gaseous precursor must diffuse against a flowing stream. The FIPER Q code is not capable of handling this transport process because it was not formulated to treat diffusion with convective flow. Therefore, it is desirable to derive an approximate analytical solution in order to determine the shape of the precursor concentration profiles in the sleeve.

Consider an idealized pore of constant radius which penetrates a graphite slab of thickness L. Let x = the distance perpendicular to the slab face and s = the distance along the pore. Now $s = \xi x$, where ξ = tortuosity of the pore. An idealized uniform circular pore with the applicable parameters and boundary conditions is shown in Fig. 4.5. In the figure x = 0 corresponds to the side of the fuel element sleeve adjacent to the fuel element purge stream and fuel compacts, while x = L corresponds to the outside of the sleeve which is in contact with the helium coolant. The helium pressure is many orders of magnitude greater than the partial pressure of fission product gaseous precursors. Thus, gas flow is directly proportional to the helium pressure gradient.

The Peach Bottom HTGR was designed so there would be a pressure gradient of He decreasing from x = L to x = 0. Thus, at the steady state in a uniform pore, the velocity of helium, V, will be in a direction opposite to the flow of fission product gases which are at a higher concentration ($C = C_o$) at x = 0 than at x = L ($C = C_L$) since their source is the fuel compacts.

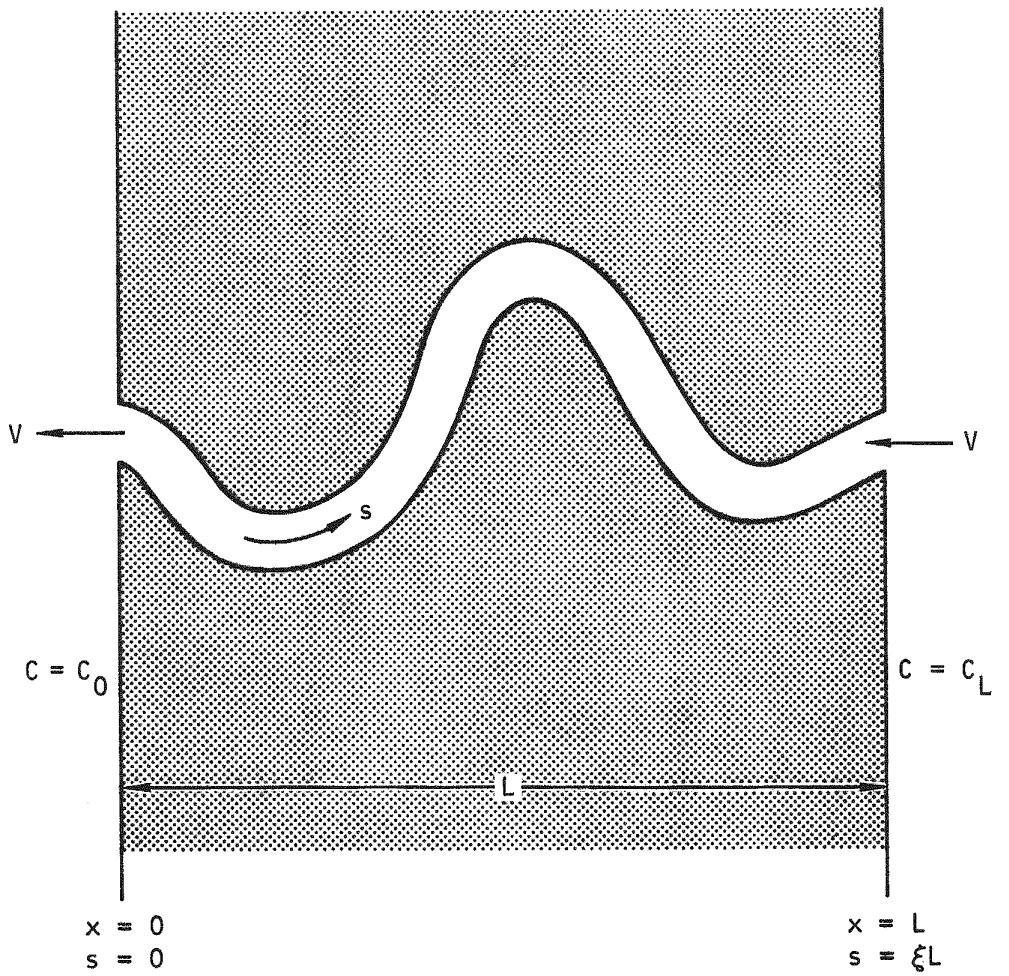

Fig. 4.5. Idealized uniform circular pore

The equation for diffusion of gaseous precursors in a given pore is

$$-\text{div } J - \lambda C = \frac{\partial C}{\partial t} \quad , \tag{4.1}$$

where the current of the gaseous precursors in the pore is

$$J = -D\frac{\partial C}{\partial s} - VC \quad . \tag{4.2}$$

The quantities s, V, and C are as defined above and D is the diffusion coefficient of the gas in the pore.

Equation 4.2 applies strictly only when

$$D_{12} << \frac{2r\bar{v}}{3} \quad ,$$

where

$D_{12} = (D^{o}_{12}/P)\ (T/273)^{1.8}$, the mutual (binary) diffusion coefficient of the gaseous precursor in helium,

D^{o}_{12} = the mutual diffusion coefficient at 1 atm total pressure and a temperature of 273°K,

P = total gas pressure (atm), which can be taken as the helium pressure,

T = absolute temperature (°K),

r = radius of idealized circular pore,

$\bar{v} = \sqrt{8RT/3M}$, the average velocity of the gas phase precursor atoms as given by the kinetic theory of gases, with R = gas constant and M = molecular weight of the precursor.

Impregnated HLM-85 Peach Bottom HTGR sleeve graphite was designed for helium backflow to be highly effective in reducing Kr and Xe diffusion through the fuel element sleeve. Tests and activity levels actually found in the

Peach Bottom HTGR coolant stream verified this (Refs. 4.2 and 4.3). Accordingly, it may be assumed that most of the precursor diffusion in the sleeve graphite occurs in larger pores where $r >> 3D_{12}/2\bar{v}$. In this case,

$$D \approx D_{12} \quad .$$

Substituting Eq. 4.2 into Eq. 4.1, we obtain the diffusion equation

$$D\frac{\partial^2 C}{\partial s^2} + V\frac{\partial C}{\partial s} - \lambda C = \frac{\partial C}{\partial t} \quad . \tag{4.3}$$

For the steady-state,

$$D\frac{d^2 C}{ds} + V\frac{dC}{ds} - \lambda C = 0 \quad . \tag{4.4}$$

To solve this, we find the roots of the auxiliary equation

$$Dp^2 + Vp - \lambda = 0 \quad , \tag{4.5}$$

which are

$$p_1 = -\left[\frac{V}{2D} + \frac{1}{2}\sqrt{\left(\frac{V}{D}\right)^2 + 4\frac{\lambda}{D}}\right] \tag{4.6}$$

and

$$p_2 = -\left[\frac{V}{2D} - \frac{1}{2}\sqrt{\left(\frac{V}{D}\right)^2 + 4\frac{\lambda}{D}}\right] \quad . \tag{4.7}$$

The solution is

$$C = K_1 \exp(p_1 s) + K_2 \exp(p_2 s) \quad , \tag{4.8}$$

where K_1 and K_2 are constants determined by the boundary conditions. For the gaseous precursors of interest in Peach Bottom fuel element sleeve graphite, the parameters are such that

$$\frac{\lambda}{D} << \left(\frac{V}{D}\right)^2 \quad .$$

For this case $P_1 \approx -V/D$ and $P_2 \approx 0$. By definition, $C = C_o$ at $x = 0$, $C = C_L$ at $x = L$, and the concentration profile for a gaseous precursor is given by

$$\frac{C}{C_o} = \exp\left(-\frac{V}{D}\xi x\right) + \left[\frac{C_L}{C_o} - \exp\left(-\frac{V}{D}\xi L\right)\right] \frac{1 - \exp\left(-\frac{V}{D}\xi X\right)}{1 - \exp\left(-\frac{V}{D}\xi L\right)} \quad . \qquad (4.9)$$

Physically, the condition given by Eq. 4.9 can be interpreted such that the mean life of the decaying radioactive species must be very much longer than the transient time of the backflowing helium across the sleeve. If this condition holds, the backflowing helium has a much greater influence on the concentration profile than the decay of the radioactive isotope.

Figure 4.6 gives concentration profiles in dimensionless units (C/C_o versus x/L). It can be seen from Eq. 4.9 that if $C_L << C_o$ and $(V/D)\xi L \geq 3$, the concentration profile is given to a good approximation by

$$C/C_o = \exp\left(-\frac{V}{D}\xi x\right) \quad . \qquad (4.10)$$

This equation applies to the sleeve concentration profiles. However, there will be a distribution of pore sizes in the sleeve graphite. Thus an observed profile, if due to the decay of precursors, will be a superposition of profiles from pores of various size.

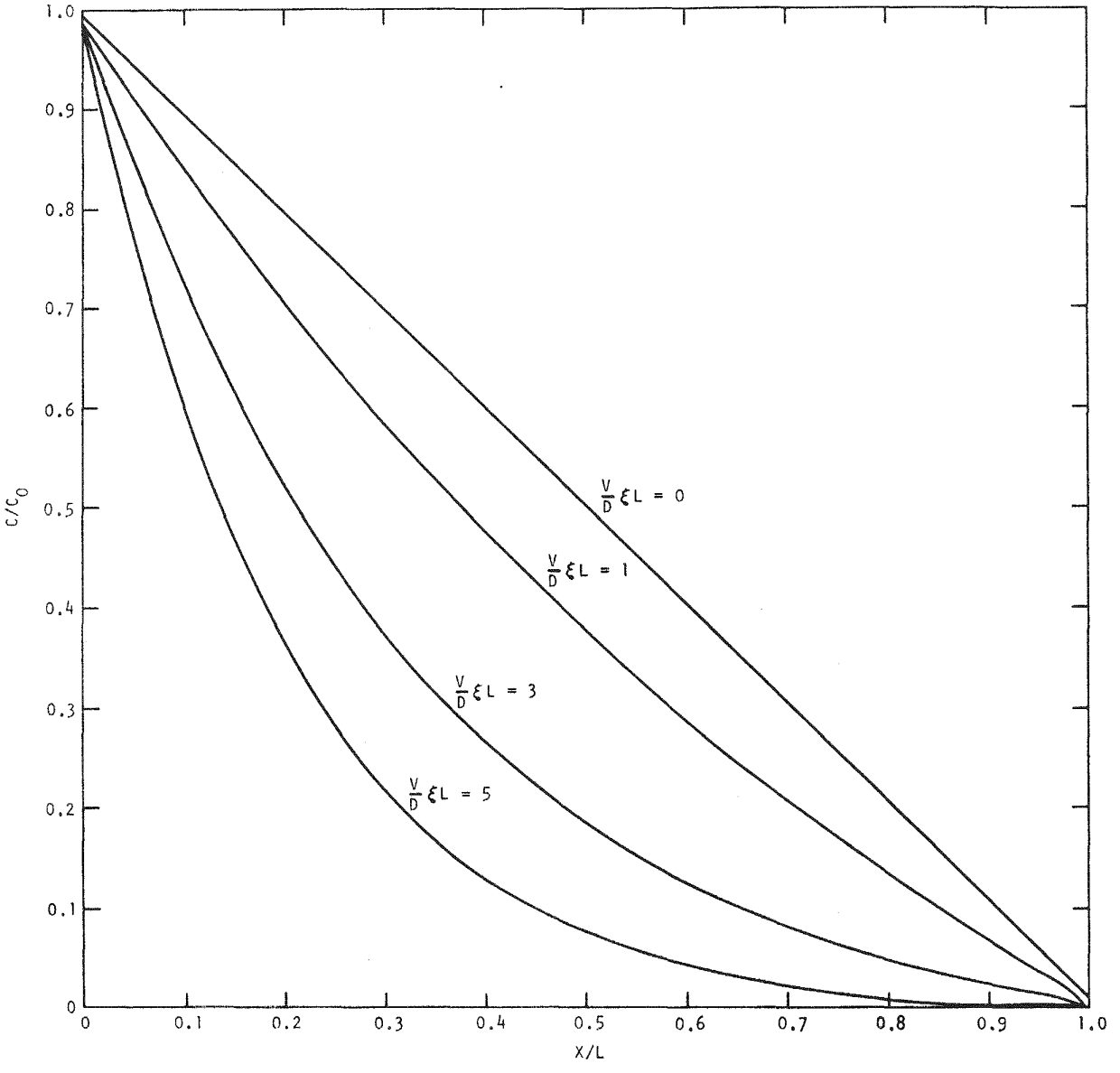

Fig. 4.6. Concentration profile of gaseous precursor as a function of backflow velocity

To justify the statement made above that

$$\frac{\lambda}{D} << \left(\frac{V}{D}\right)^2$$

the value of V/D can be estimated from data given in Refs. 4.2 and 4.3. It is assumed that the idealized uniform circular pore model of Fig. 4.5 applies.

Differentiating and substituting Eq. 4.9 into Eq. 4.2 gives

$$J = \frac{C_o V}{\exp\left(\frac{V}{D}\right)\xi L - 1} \tag{4.11}$$

when $C_L << C_o$. Equation 4.11 represents the current of diffusing precursor gas atoms through a pore when there is backflow of helium gas in the pore.

The transport coefficient for the diffusing gas molecules for these conditions is defined as

$$K = \frac{J\xi L}{C_o} = \frac{V\xi L}{\exp\left(\frac{V}{D}\right)\xi L - 1} \quad . \tag{4.12}$$

The limit as $V \to 0$ in Eq. 4.12 is $K = D$. The current (or flux) ratio is therefore

$$\frac{J(V)}{J(0)} = \frac{K}{D}\frac{\frac{V}{D}\xi L}{\exp\left(\frac{V}{D}\right)\xi L - 1} \quad . \tag{4.13}$$

In a porous material, K and D are reduced due to the fact that the pores occupy only a fraction of the total area. However, the reduction in K and D is in the same proportion to give K_{eff} and D_{eff}; therefore, for the idealized uniform pore model,

$$\frac{K_{eff}}{D_{eff}} = \frac{K}{D} = \frac{x}{e^x - 1} \qquad (4.14)$$

where

$$x = \frac{V}{D}\xi L \quad .$$

We now calculate x taking $K_{eff} = 7 \times 10^{-7}$ cm^2/sec as given in Ref. 4.3 for xenon release into the Peach Bottom primary coolant. The value of D_{eff} is 1.6×10^{-5} cm^2/sec and was obtained from Fig. 9 in Ref. 4.2. For xenon, at Peach Bottom operating conditions of 23.8 atm of helium pressure and a typical sleeve temperature of 1000°K,

$$D_{eff} = \frac{1.6 \times 10^{-5}}{23.8} \quad \frac{1000}{300} = 5.8 \times 10^{-6} \quad .$$

Thus, at reactor conditions,

$$\frac{K_{eff}}{D_{eff}} = \frac{7 \times 10^{-7}}{5.8 \times 10^{-6}} = \frac{1}{8.35} \quad .$$

Substituting into Eq. 4.14,

$$\frac{e^x - 1}{x} = 8.35$$

and

$$x = \frac{V}{D}\xi L = 3.37 \quad .$$

The thickness of the Peach Bottom sleeve is L = 0.93 cm. The tortuosity of the sleeve graphite is assumed to be 3, i.e., $\xi = 3$. Sometimes higher tortuosities ($\xi = 10$) are estimated, but these include the effect of blind-ended pores and have questionable physical reality. For a bed of pack spheres, $\xi = \sqrt{2}$. Substituting these values gives

$$\frac{V}{D} = \frac{3.37}{3\ (0.93)} = 1.21 \quad .$$

The value of V/D can now be compared to λ/D. The decay constant for Xe-137 is $\lambda = 4.1 \times 10^{-3}\ sec^{-1}$. For Xe diffusing in helium at 1000°K and 350 psia, D = 0.175 cm^2/sec (calculated from formula in Ref. 4.4). The decay constant of Xe-133, the precursor of Cs-134, is even smaller. Thus, $\lambda/D << V/D$. It is concluded that Eq. 4.9 is a good approximation to the solution of the steady-state transport equation (Eq. 4.5) and the concentration profile is independent of half-life.

Curves calculated using Eq. 4.9 are plotted along with the FIPER calculated curves in Figs. 4.1 through 4.4. The most striking conclusion is that the curves representative of flow and decay of a precursor and metal diffusion have similar shapes (see Fig. 4.3, for example). In none of the four sleeve positions at which concentration profiles were obtained is there a clear indication that a section of the profile is due solely to the metal component or gaseous component, as was the case for the spine data. Therefore, the precursor contribution could not be subtracted from the profiles to give a metal component, and no cesium metal diffusion coefficients were obtained for the sleeve.

Comparison of Cesium Diffusion Coefficient Data for Peach Bottom Spine Graphite With Other Data

Diffusion coefficients for cesium in graphite have been derived previously from laboratory studies and from postirradiation analyses of concentration profiles. Frequently, there is disagreement between the two methods of determining diffusion coefficients because of the difficulty

in duplicating in-pile conditions in the laboratory. Flowers et al., in a paper that summarizes British experimental results (Ref. 4.5), report diffusion coefficients measured in the laboratory to be orders of magnitude larger than in-pile determinations. The anomaly is attributed to concentration effects and to gradual diffusion into graphite grains during long-term irradiations, occuring simultaneously with relatively rapid diffusion between grains. Diffusion into grains does not significantly occur in short-term laboratory experiments.

Variation of cesium diffusion coefficients with concentration has been reported by Flowers (Ref. 4.6). At concentration levels around 1 μg/g C, the diffusion coefficient data are described by the equation

$$\log_{10} D = 0.19 - \frac{10390}{T} \quad .$$

At concentration levels in the range 100 to 1000 μg/g C, the data are described by the equation

$$\log_{10} D = -1.158 - \frac{3940}{T} \quad .$$

Cesium diffusion coefficients described by the two equations differ by more than three orders of magnitude at 1000°C. Data representing diffusion at low concentration in a Dragon fuel tube agree well with the data obtained from the Peach Bottom D13-05 spine analysis. At concentration levels representative of the D13-05 analysis, cesium diffusion coefficient dependence on concentration is not thought to be significant. Bromley et al. (Refs. 4.7, 4.8) and Riedinger (Ref. 4.9) have also reported cesium diffusion coefficients at high concentrations.

The value of the cesium diffusion coefficient is also dependent on the type of graphite. It has been reported that the cesium diffusion coefficient for graphite matrix material has a higher value by an order of magnitude than nuclear structural graphite (Ref. 4.5).

Figure 4.7 compares diffusion coefficient data from the D13-05 spine analyses and data from analyses of other in-pile experiments. It is maintained that in-pile experiments give a more accurate description of cesium diffusion than laboratory (out-of-pile) experiments because of the difficulty of reproducing in-pile conditions in the laboratory. The current reference cesium diffusion coefficient data for cesium in graphite were obtained from the laboratory work of Bryant et al. (Ref. 4.10). A curve (dashed line) representative of these data is included in Fig. 4.7. Bryant's out-of-pile experiments were conducted with graphite and at temperatures which are not representative of reactor conditions.

The British have performed many postirradiation examinations of Dragon fuel tubes (Refs. 4.11 through 4.18) and the diffusion coefficient data which summarize their results (Ref. 4.5) are plotted in Fig. 4.7. In plotting the data from the D13-05 spine analyses, average no-gap temperatures were used (see Table 4.4 in the previous Quarterly Progress Report, Gulf-GA-A12422).

Included in Fig. 4.7 are some previously unpublished GGA diffusion coefficient values obtained from cesium diffusion profiles found in the postirradiation chemical examination of GAIL IV fuel element (Ref. 4.19). The movement of control rods caused large axial variations in temperature over much of the GAIL IV fuel element, especially for corings 1, 3, 4, and 13. Therefore, diffusion coefficient data for these corings are not plotted in Fig. 4.7. The data obtained from the GAIL IV cesium profiles are given in Table 4.1.

A least squares fit of the in-pile data is represented by the solid line in Fig. 4.7. The activation energy obtained from the slope of this line is 29.2 kcal/mole. This activation energy is very near that determined from D13-05 data alone, 27 kcal/mole.

FISSION PRODUCT DEPOSITION LOOP STUDIES

Work on the fission product deposition loop has continued. During this quarter blowdown tests were completed and wipedown tests were conducted on

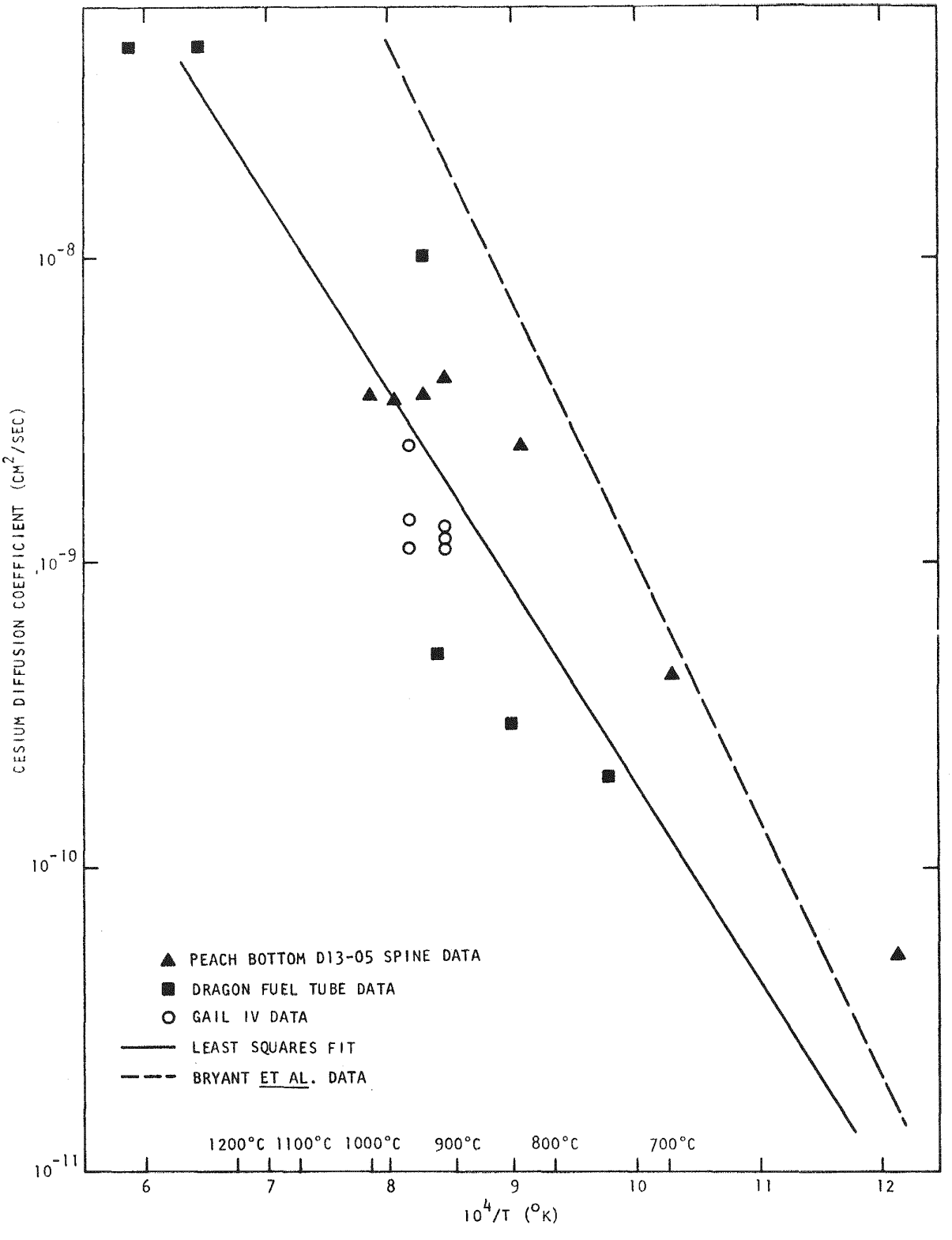

Fig. 4.7. Diffusion coefficients for cesium in graphite determined from fuel element concentration profile analyses

TABLE 4.1
DIFFUSION COEFFICIENTS FOR CESIUM (D_{Cs})
IN SPEER 780-S GRAPHITE BASED ON GAIL IV
FUEL ELEMENT CESIUM PROFILES

Isotope	Coring Number	Estimated Temperature (°C)	C_o (mg Cs/g C)	D_{Cs} (cm^2/sec)
137	1	640	6.2×10^{-6}	2.8×10^{-10}
137	1	640	5.6×10^{-6}	1.10×10^{-9}
137	3	640	6.8×10^{-4}	3.2×10^{-10}
137	3	640	5.9×10^{-4}	8.4×10^{-10}
134	3	640	2.6×10^{-6}	4.2×10^{-10}
137	4	770	3.5×10^{-4}	3.6×10^{-10}
134	5	910	5.0×10^{-5}	1.08×10^{-9}
137	5	910	4.5×10^{-5}	1.18×10^{-9}
134	7	910	---	1.19×10^{-9}
137	7	910	---	1.31×10^{-9}
137	9	950	6.3×10^{-3}	1.12×10^{-9}
134	9	950	1.05×10^{-4}	1.38×10^{-9}
134	11	950	3.4×10^{-6}	2.4×10^{-9}
137	11	950	4.6×10^{-4}	2.4×10^{-9}
134	13	870	2.9×10^{-5}	5.8×10^{-9}
137	13	870	2.5×10^{-3}	1.7×10^{-9}

samples from the third loop experiment. The fourth deposition loop experiment was also conducted.

The objectives of this work are to obtain plateout distribution data and to obtain liftoff (or blowdown) data by subjecting sections of the loop to conditions of higher surface shear forces than obtained in the normal operating loop. The plateout data are used to test and refine the PAD code, which was developed at GGA for predicting the fission product plateout distribution in an HTGR primary coolant circuit. The liftoff data are valuable for use in safety analyses associated with the hypothetical depressurization accident.

The blowdown results of the third loop experiment are given in Fig. 4.8. As indicated, less than 2% of the deposited iodine was blown off for shear ratios up to 10. Although the scatter in blowdown data is large, the average values, represented by the data points, indicate an increasing blowdown fraction with increasing shear ratio.

Wipedown tests were conducted on six samples from the third deposition loop experiment. Four of the samples were at the entrance or exit of the loop, and approximately 50% of the surface activity was removed by wiping down the surface with hand pressure force. Wipedown tests on two samples away from the entrance or exit of the loop resulted in approximately 25% of the surface activity being removed. It is considered that these wipedown tests represent an estimate of the fraction of the deposited material that is on particulate material or on a removable film. Additional wipedown tests are planned for the fourth loop experiment to investigate the wipedown results as a function of position in the loop.

The fourth deposition loop experiment is in progress. The loop has been successfully operated and the plateout results are currently being analyzed. Cesium, tagged with Cs-137, was the depositing species. This loop did not have the chilled section and hence operated at higher and near constant temperatures. The loop surface temperatures ranged from approximately 400°C (750°F) to 315°C (600°F). With the near-isothermal operating conditions, this loop experiment is expected to be most valuable for checking the PAD code.

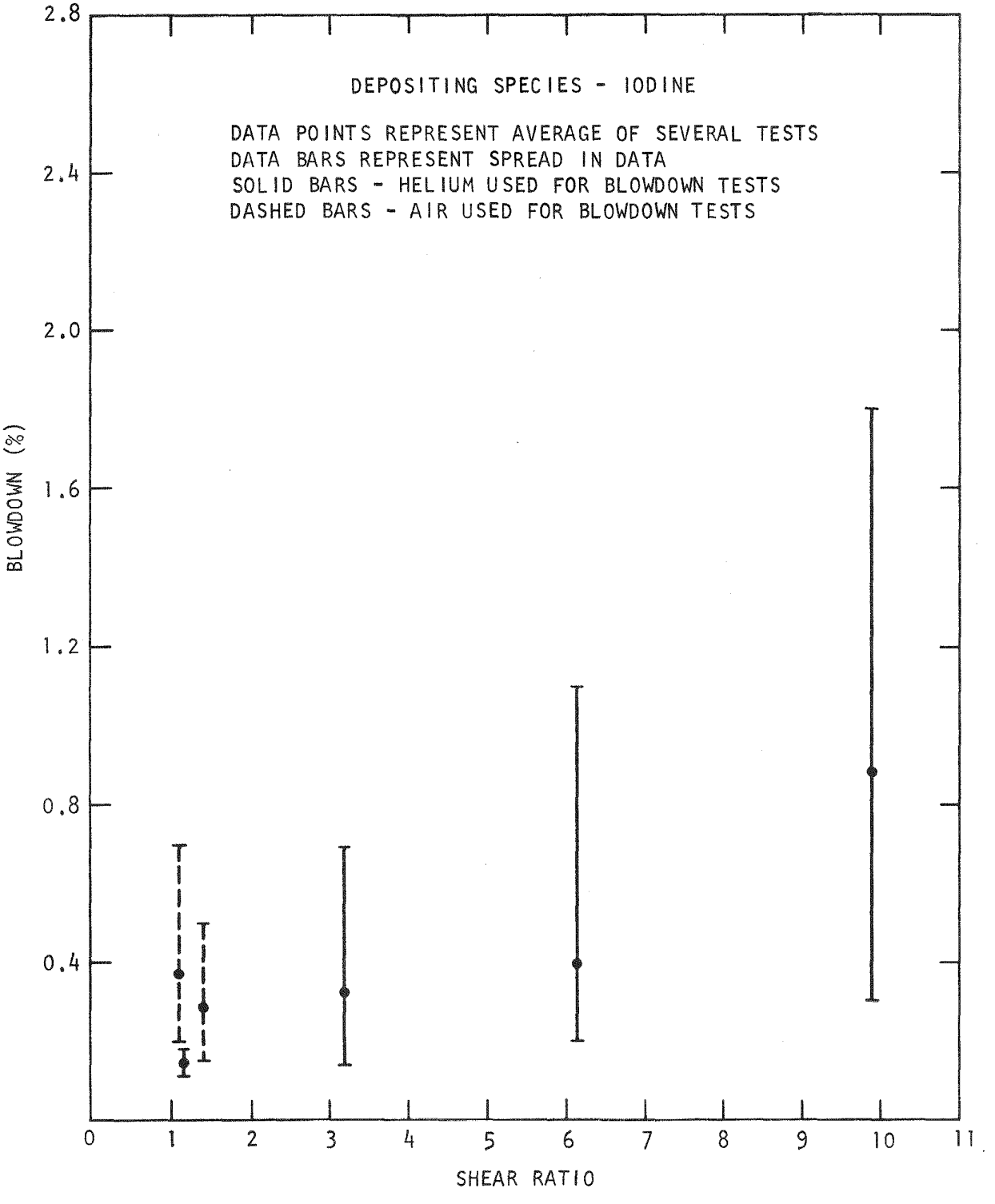

Fig. 4.8. Blowdown results for third deposition loop experiment

VAPOR PRESSURE STUDIES

The vapor pressure of cesium sorbed on H-327 graphite is being studied using the Knudsen cell mass spectrometric method. The objective of this work is to extend the vapor pressure data to low concentrations (below 10 ppm), comparable to presently predicted end-of-life concentrations of cesium in fuel element graphite at the graphite-helium interface. The low concentration data are important for use in refining predicted releases of cesium nuclides in HTGR systems.

These studies have yielded a surprising result. The vapor pressure data (or isotherms) have shown a downward pressure break at about 5 ppm cesium.

A systematic investigation has been directed toward determining if this pressure break is the result of an experimental artifact. Areas of investigation have included sample size, Knudsen cell hole size, cesium takeup by the Knudsen cell, pretreatment of the sample, impurities in the starting graphite, analytical errors, and lower temperature experiments. Apparently, none of these, as studied, have been responsible for the pressure break. The results of a recent isothermal run in which the cesium-H-327 graphite sample was contained in a pyrolytic carbon cup inside a molybdenum Knudsen cell have been analyzed. (Normally the sample is contained in the molybdenum cell only.) The downward pressure break in the cesium isotherm was unaffected, occurring at approximately 5 ppm cesium. At this time, it appears reasonable, therefore, to assign the pressure break to the cesium-H-327 graphite system itself and not to an artifact of the experimental procedure.

If continued studies demonstrate that this pressure break is real, it can lead to a significant reduction in the predicted release of cesium nuclides in HTGR systems.

REACTION OF STEAM WITH GRAPHITE

The effect of helium pressure on the reaction rate of H-327 graphite with steam is being measured over the range 800° to 1000°C, utilizing pressures from 15 to 715 psia. The purpose of this work is to quantitatively determine the overall reaction rate of the steam-graphite reaction as a function of helium pressure for comparison with theoretical preductions. The data are needed for use in calculations to predict the consequences of a steam in-leakage accident.

Apparatus for use in performing the steam-graphite studies was assembled in the fall of 1972. Safety approval was obtained. The apparatus was first operated successfully in December 1972. Preliminary data were scattered and the apparatus was extensively modified. Recent results are much more consistent than the earlier data and are considered to be reliable. The data were measured at temperatures of 900° and 1000°C and helium pressures of 15 to 415 psia. The results indicate a drop in reaction rate that is in reasonable agreement with theoretical predictions.

Apparatus and Procedure

The reaction rate studies are carried out in a high-pressure double-chamber furnace (Fig. 4.9), capable of maintaining temperatures beyond 1000°C at helium pressures up to 750 psi. The inner and outer chambers are separated by a closed tube of Inconel 625, a material characterized by high strength and low oxidation at high temperatures. The inner chamber contains the carbon sample and is so designed that the incoming high-pressure helium-steam mixture is first heated and then passed upward over the hot graphite sample. The outer chamber contains a resistance heater with suitable insulation and is independently pressurized with helium to maintain a near-zero pressure gradient across the Inconel chamber wall. The absolute pressure within the furnace and any pressure differential existing between the inner and outer chambers are continuously monitored with absolute and differential pressure gauges, respectively.

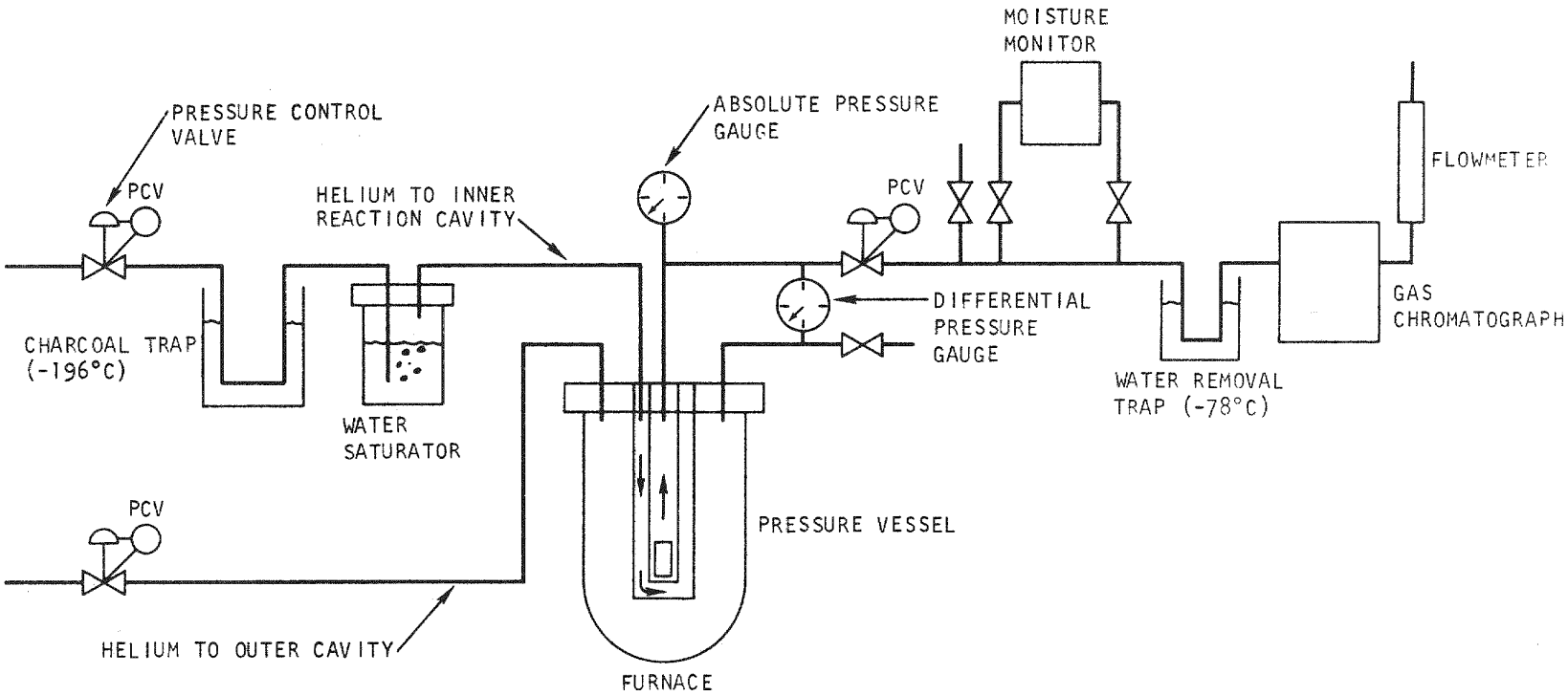

Fig. 4.9. High-pressure steam-graphite apparatus

Prior to entering the inner chamber of the furnace, the high-pressure helium is passed through a charcoal trap maintained at -196°C to remove traces of oxygen. The helium is then saturated with water vapor at room temperature in a high-pressure saturator. After exiting from the furnace, the low-pressure gas mixture is passed through a cold trap maintained at -78°C to remove excess water vapor present after reaction. The dry gas is then introduced into a gas chromatograph, where the quantities of carbon monoxide and carbon dioxide produced under steady-state conditions are determined. With these data and the weight of the graphite sample, the reaction rate as a function of helium pressure can be calculated.

Results

Initial reaction rate data are shown in Table 4.2.

TABLE 4.2
EFFECT OF HELIUM PRESSURE ON RATE OF REACTION OF H-327 GRAPHITE WITH STEAM

Temperature (°C)	Pressure (psia)	Reaction Rate (%/hr)
900	15	2.50×10^{-3}
900	115	1.66×10^{-3}
900	215	1.23×10^{-3}
900	315	1.07×10^{-3}
900	415	1.05×10^{-3}
1000	15	1.45×10^{-2}
1000	115	9.76×10^{-3}
1000	215	7.75×10^{-3}
1000	315	5.42×10^{-3}
1000	415	3.55×10^{-3}

The results indicate a rapid dropoff of reaction rate with rising helium pressure, in reasonable agreement with theoretical predictions for heterogenous reactions involving porous material. An increase in helium pressure

should effectively reduce the in-pore diffusion of steam, and the overall reaction rate should diminish as a function of the inverse square root of the helium pressure. It should be noted that the graphite sample used had undergone no burnoff prior to introduction into the high-pressure furnace.

Following these measurements, several improvements have been introduced into the apparatus in order to extend the results and reduce data scatter. A new water saturator, capable of withstanding pressures up to 750 psi has been added, the previous saturator being limited to 450 psi. In addition, a moisture monitor will be utilized to verify predicted steam concentrations and to assure that steam saturation has been achieved. Finally, an improved temperature controller has been introduced to more precisely maintain reaction temperature. This is necessary as the reaction rate is strongly affected by small variations in furnace temperature.

REFERENCES

4.1 Forutanpour, B., and B. Roos, "FIPER X, A Fortran V Program for the Solution of One-Dimensional Linear and Non-Linear Diffusion Problems," USAEC Report GA-9904, Gulf General Atomic, 1969.

4.2 Riedinger, A., "Gas Transport Properties and Pore Structure of Some Nuclear Graphites," USAEC Informal Report GAMD-4814, General Dynamics, General Atomic Division, June 1964.

4.3 Lofing, D. R., E. E. Anderson, and W. E. Bell, "Fission Product Control and Fuel Element Release at Peach Bottom HTGR Nuclear Power Station," USAEC Report GAMD-7904, Gulf General Atomic, July 1972.

4.4 Treybal, R. E., Mass Transfer Operations, 2nd Edition, McGraw-Hill, New York (1968), p. 25, formula 2.37.

4.5 Flowers, R. H., J. B. Sayers, and M. S. T. Price, "The Present State of Data in the Safety Analysis of the HTGR," paper presented at the Safety Aspects of High-Temperature Reactor Systems Conference, Paris, November 24-25, 1971, Paper 16.

4.6 Flowers, R. H., "The Relationship of Fission Product Release Limitations to the Design and Operation of a Large HTR Station," Proc. Gas-Cooled Reactor Information Meeting, ORNL, April 27-30, 1970, USAEC Report Conf. 700401 (TID-4500).

4.7 Bromley, J., and N. R. Large, "The Migration of Fission Products in Artificial Graphite," Proc. Fifth Conference on Carbon, Vol. 1 Pergamon Press, New York (1962), p. 365.

4.8 Bromley, J., A. H. Paddon, and N. Moul, "The Diffusion of Cesium, Strontium and Barium Through Porous Graphites," United Kingdom Atomic Energy Report AERE-R-3471, April 1961.

4.9 Riedinger, A. B., C. E. Milstead, and L. R. Zumwalt, "Experiments on the Diffusion of Cesium and Barium Through Graphites of Low Helium Permeability," Proc. Fifth Carbon Conference, Vol. 2, Pergamon Press, New York (1963), p. 405.

4.10 Bryant, E. A., et al., "Rates and Mechanisms of the Loss of Fission Products from Uranium - Graphite Materials," Nucl. Sci. Eng. 15, 288 (1963).

4.11 Barr, P., et al., "The High Temperature Experiment in Dragon Charge 2, Pt. II: Operation of the Irradiation Experiment and Postirradiation Evaluation," United Kingdom Atomic Energy Report DPR-623, 1969.

4.12 Barr, P., et al., "A Study of Fission Product Release from Compacted Uranium/Thorium Coated Particle Fuel, United Kingdom Atomic Energy Report DPR-682, 1969.

4.13 Brown, P. E., et al., "Fission Products in Dragon Fuel Rod 000-7," United Kingdom Atomic Energy Report AERE-R-5651, 1968.

4.14 Groos, E., and H. J. de Nordwall, "Postirradiation Radiochemical Analysis of the Loop Pluto IIIA," United Kingdom Atomic Energy Report AERE-R-4434, 1964.

4.15 Brown, P. E., and H. J. de Nordwall, "Postirradiation Radiochemical Analysis of Charge 8 for Pluto Loop 'A'," United Kingdom Atomic Energy Report AERE-R-5040, 1965.

4.16 de Nordwall, H. J., et al., "Postirradiation Radiochemical Analysis of Charge 15 of Pluto Loop A." United Kingdom Atomic Energy Report AERE-R-5404, 1967.

4.17 de Nordwall, H. J., et al., "Postirradiation Radiochemical Analysis of Pluto Loop A Charge 16," United Kingdom Atomic Energy Report AERE-R-5405, 1967.

4.18 Baker, H. T., et al., "Fission Products in the Dragon Charge II Centre Rod Elements Nos. 414, 417, 430, and 431," United Kingdom Atomic Energy Report DW(71)4.

4.19 Bell, W. E., E. E. Anderson, and C. E. Milstead, "Postirradiation Chemical Examination of the GAIL IV Fuel Element," USAEC Report GA-8588, Gulf General Atomic, June 1968.

TASK V
RECYCLE FUEL STUDIES

HTGR FUEL RECYCLE PLANT STUDY

Equipment sizing for plants capable of handling 15,000-, 30,000-, or 45,000-MW(e) economies is continuing. The effort is about 70% complete.

Preliminary plant layouts have been prepared for the 45,000-MW(e) plant (see Fig. 5.1). The design philosophy utilized in these layouts is to divide the process areas of the plant into wet and dry areas to take advantage of the larger equipment possible in dry areas. Process areas that will be kept dry are: cask unloading and loading areas, fuel storage areas, crushing cells, burner cells, coater cells, rod fabrication, and block assembly. These areas will be serviced by a dry ventilation system and will be separated from wet areas by dry moats or corridors. Dry cells will not be serviced by any water lines, and cooling where necessary will be provided by gases or a nonaqueous system.

Guidelines for the study are being changed to permit recycle U-235 fissile fuels to be fabricated and assembled in an unshielded facility, such as a fresh fuel plant. Shipping considerations suggest that fuel kernels be prepared at the refabrication site and then shipped for further fabrication to a fresh fuel plant elsewhere. Assuming a crossover of 0.1% U-233 results in less than 0.5 ppm U-232 in the U-235, and unshielded fabrication will be possible.

The ANSI subcommittee work to develop a standard for an irradiated fuel receiving and storage facility is continuing. The standard is being prepared to cover both wet and dry storage of fuel.

Criticality Studies

An extensive set of survey calculations for particle coater and fluidized bed burner development studies has been completed. The results of these studies should provide sufficient information to determine the constraints that will be imposed by criticality considerations on the design of the HTGR fuel reprocessing plant.

Criticality calculations were performed for fully reflected cylinders of $U^{233}O_2$ and ThO_2. Thorium/uranium ratios of 0, 4, and 10 were considered. Moderation with water and carbon was included. The degree of moderation was varied from none to full as characterized by H/U ratios from 0 to 1000 and C/U ratios from 0 to 5000.

The MICROX spectrum code (Ref. 5.1) was used to generate P_1 transport theory cross sections with nine energy groups for each different case. These cross sections were used in the 1DFX one-dimensional discrete ordinate multigroup transport theory code (Ref. 5.2) to generate criticality data. The critical height for a fixed-diameter cylinder was determined by using the 1DFX axial search option. The critical mass of the cylinder is determined by its height, diameter, and material composition. At each diameter several different compositions were used, a curve of critical mass versus uranium density was constructed, and the minimum critical mass at that diameter was determined. This procedure was repeated for cylinders of several diameters, and a curve of minimum critical mass versus cylinder diameter was constructed. This procedure was followed for all mixtures: Th/U = 0, 4, and 10 with carbon moderation and with water moderation. Except where noted, full water reflection on the sides and ends of the cylinders was assumed. The critical mass versus cylinder diameter curves are shown in Figs. 5.2 through 5.7.

Particle coater designs from 4 in. to 25 in. in diameter were considered. Fluidized bed burner designs up to 70 in. in diameter were included. If internal water flooding of the cylinders is considered credible, the operating mass limits are constrained to very small values, generally

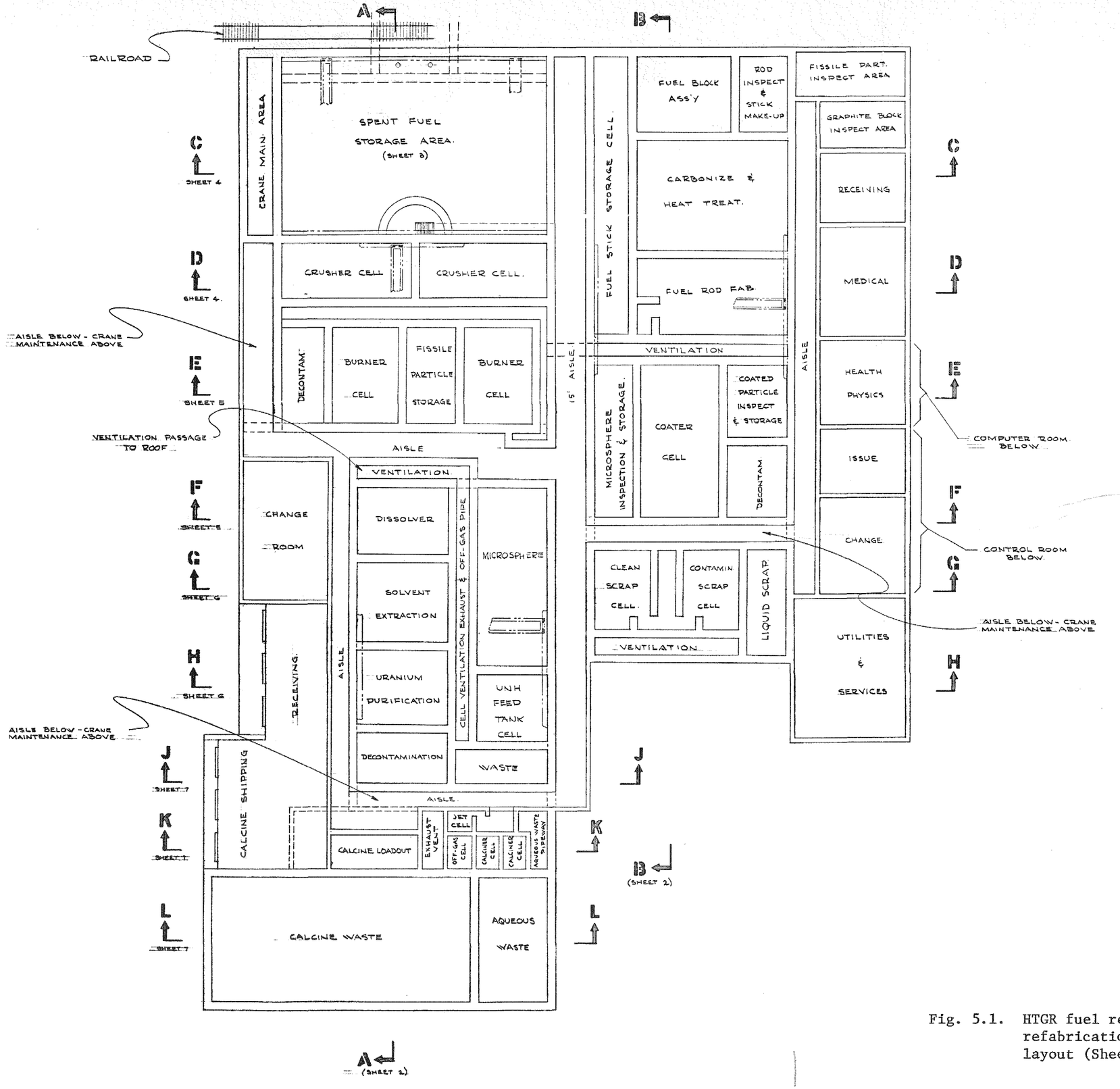

Fig. 5.1. HTGR fuel reprocessing-refabrication plant layout (Sheet 1 of 3)

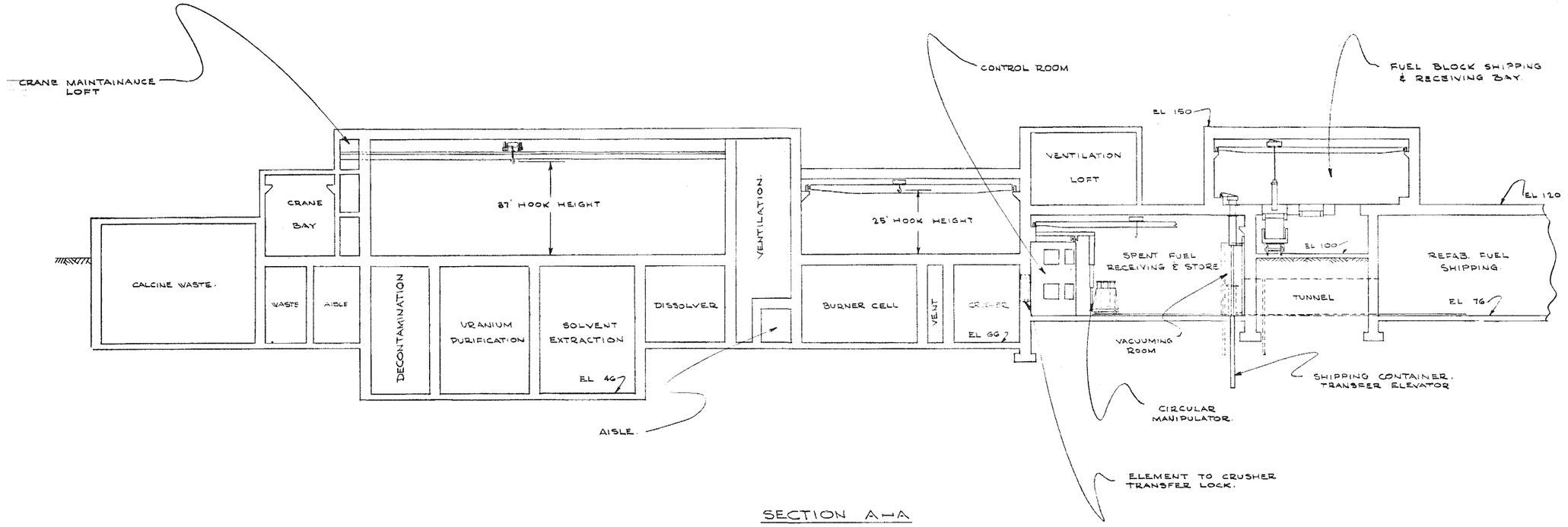

SECTION A-A

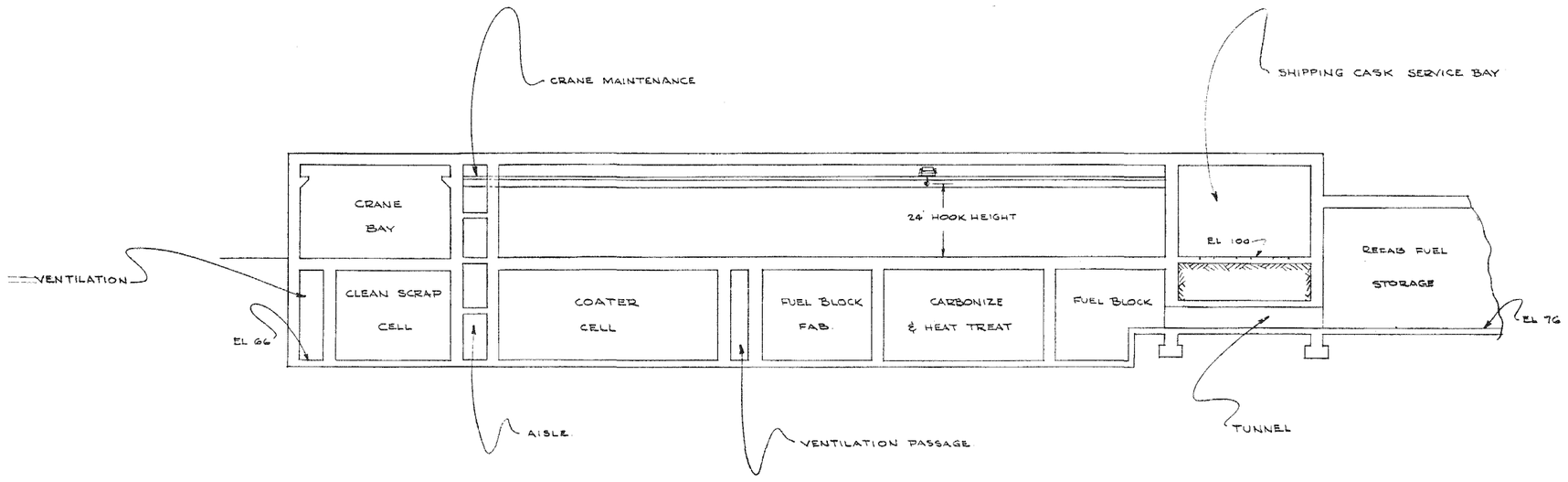

SECTION B-B

Fig. 5.1. HTGR fuel reprocessing-refabrication plant layout (Sheet 2 of 3)

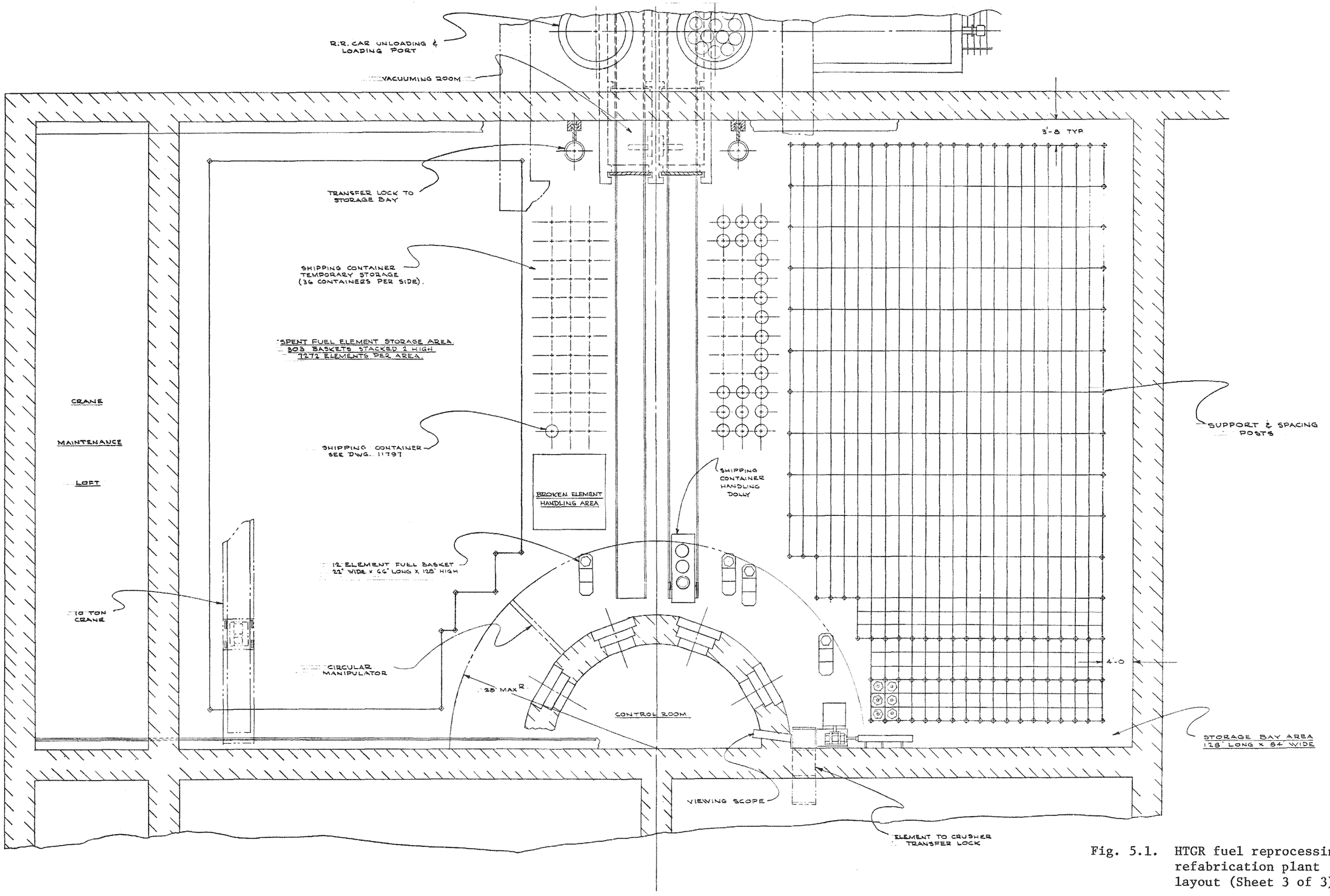

Fig. 5.1. HTGR fuel reprocessing-refabrication plant layout (Sheet 3 of 3)

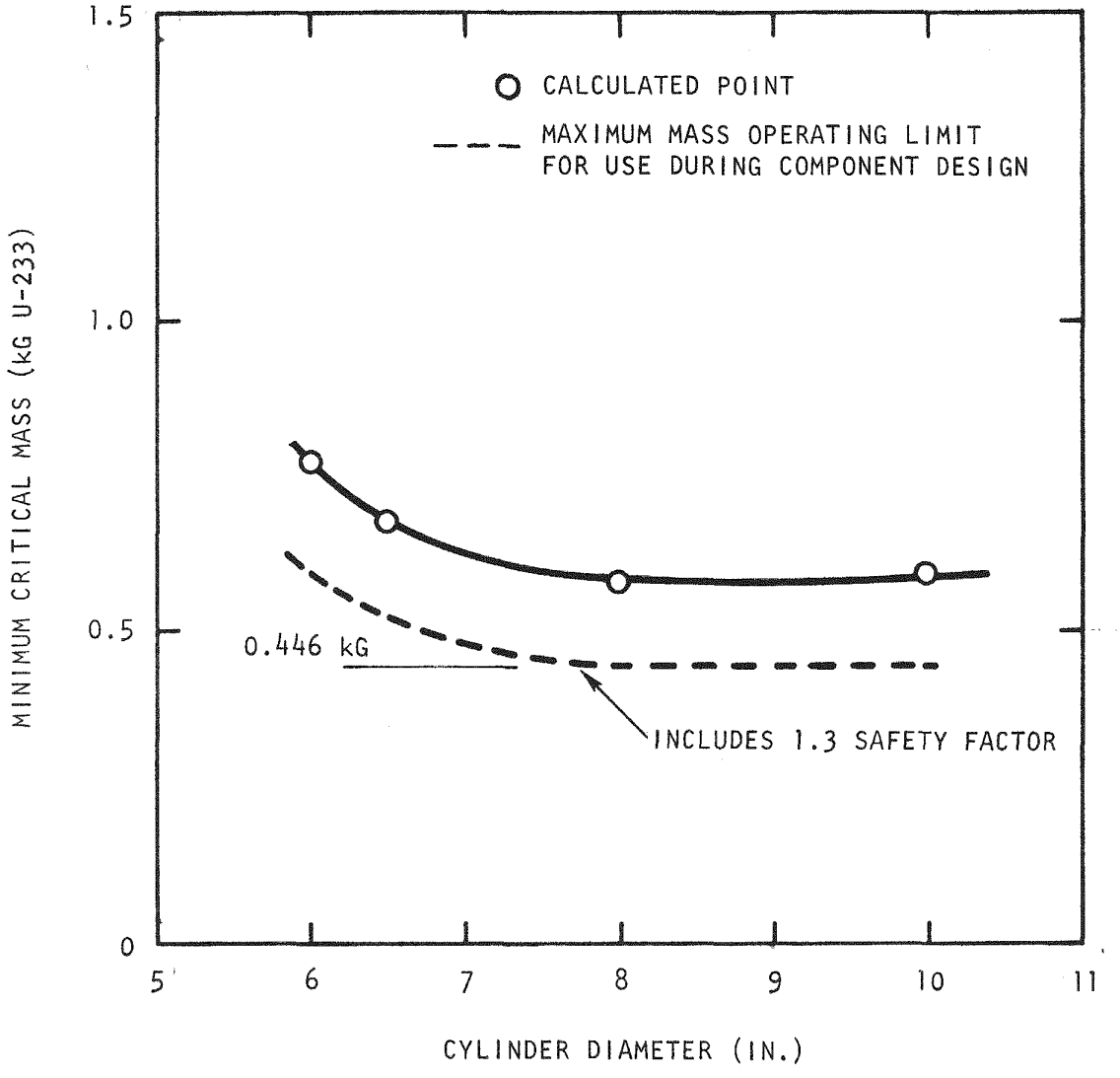

Fig. 5.2. Critical mass versus cylinder diameter, water moderated, Th/U = 0

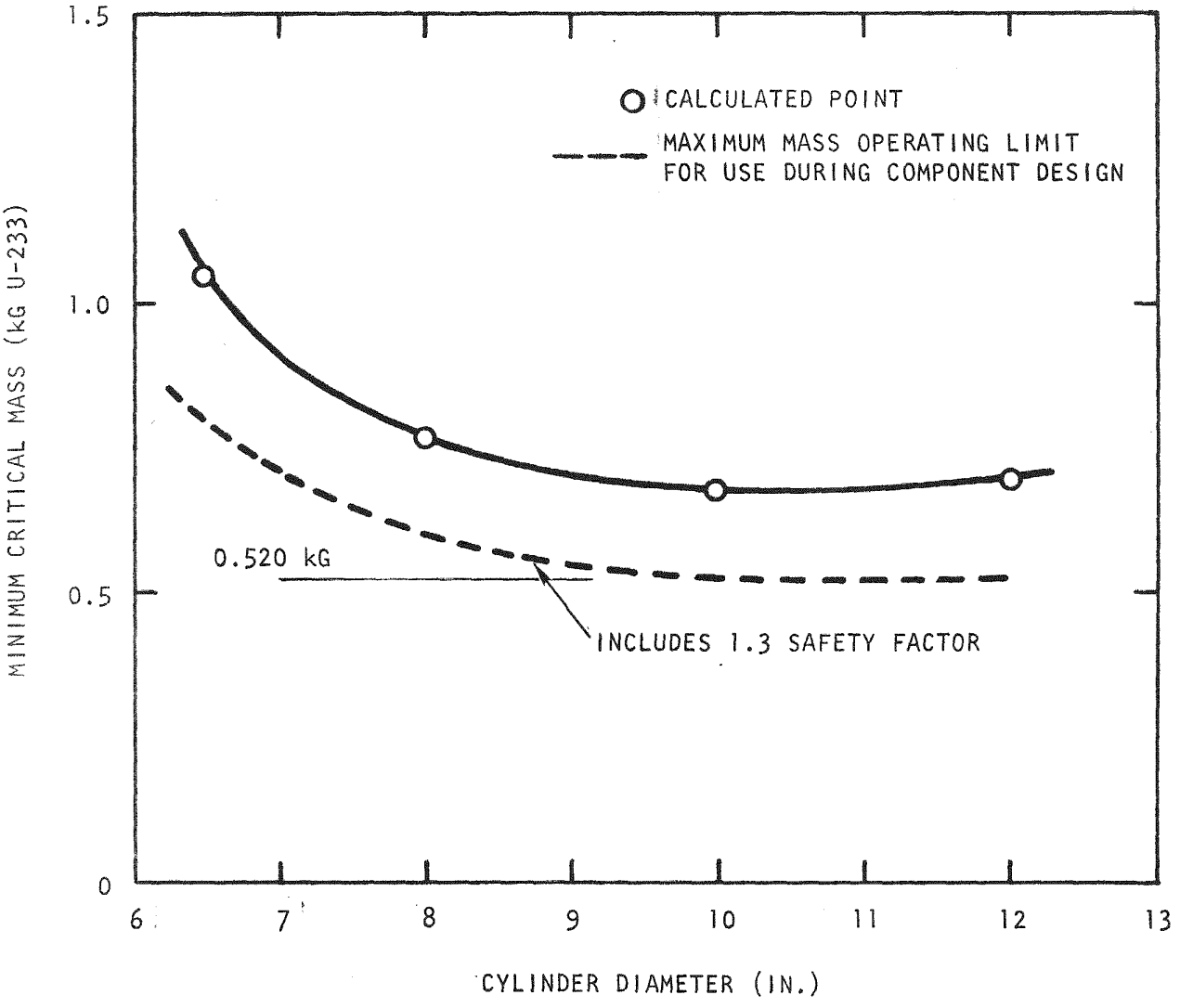

Fig. 5.3. Critical mass versus cylinder diameter, water moderated, Th/U = 4

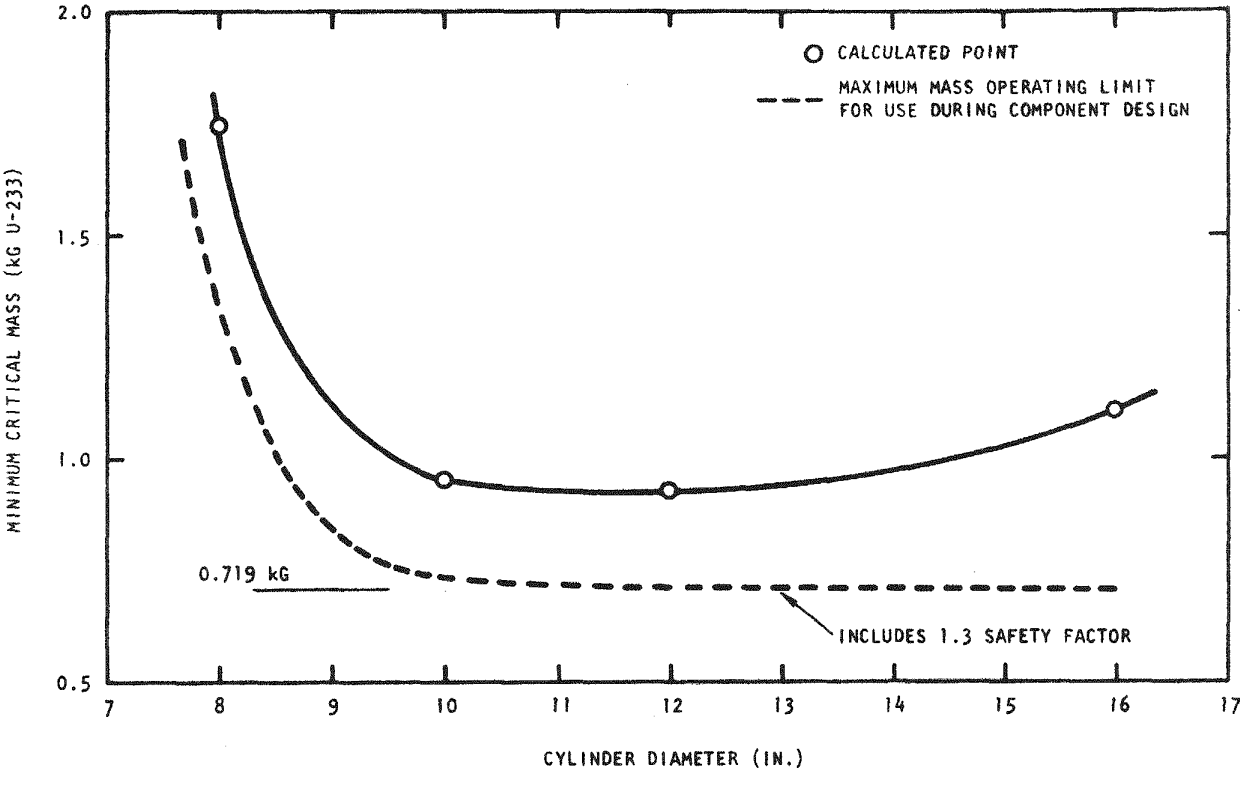

Fig. 5.4. Critical mass versus cylinder diameter, water moderated, Th/U = 10

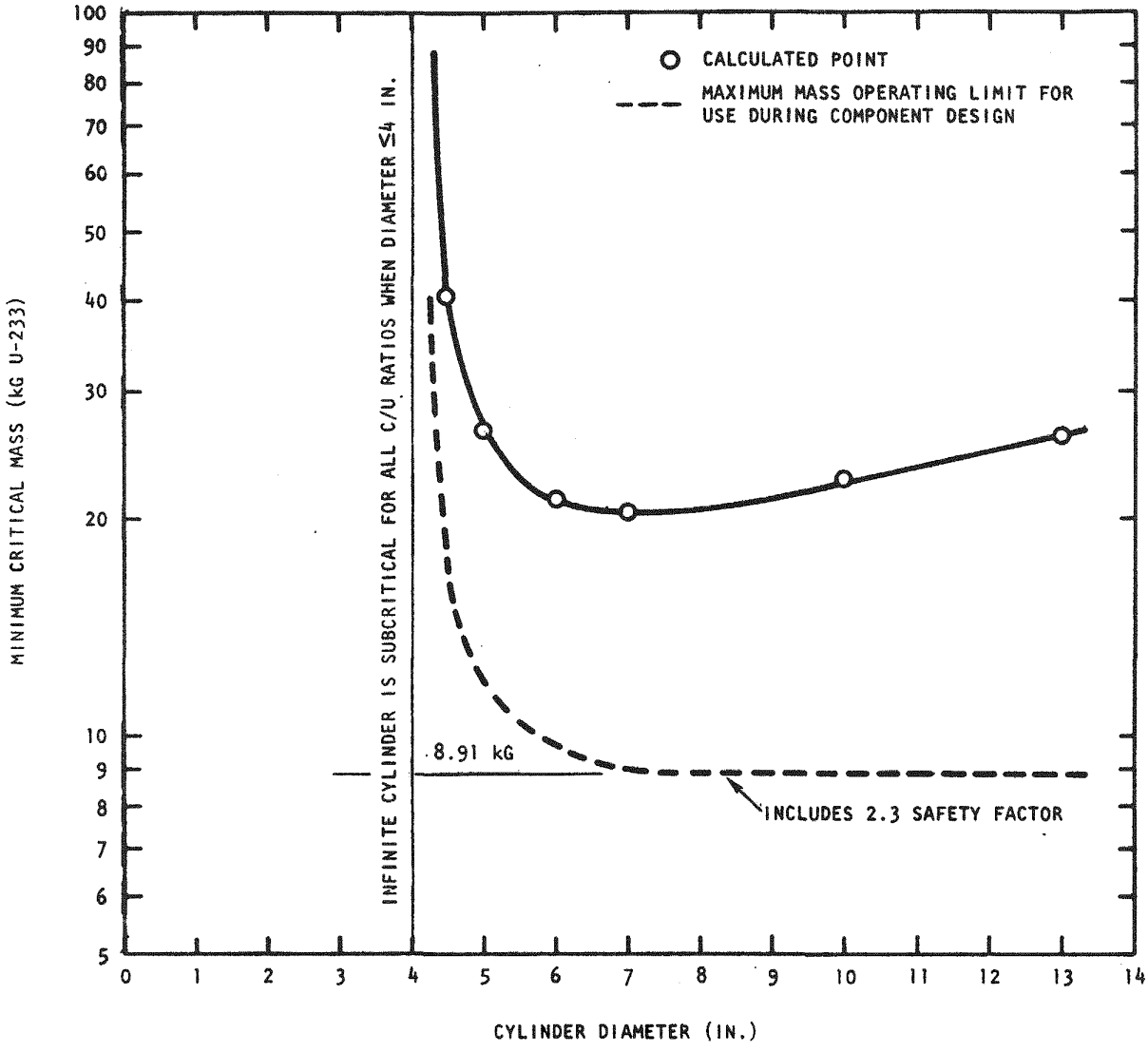

Fig. 5.5. Critical mass versus cylinder diameter, graphite moderated, Th/U = 0

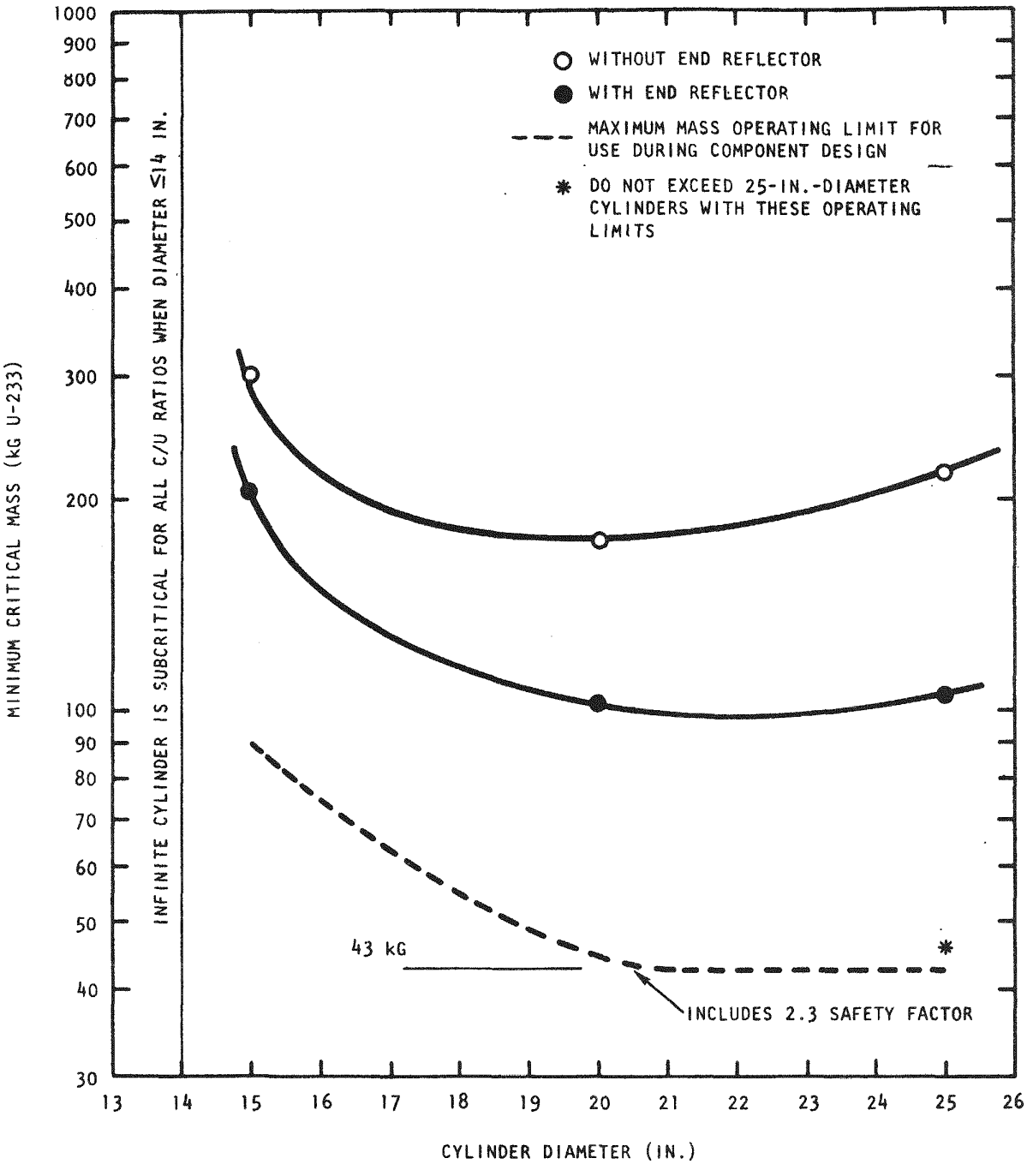

Fig. 5.6. Critical mass versus cylinder diameter, graphite moderated, Th/U = 4

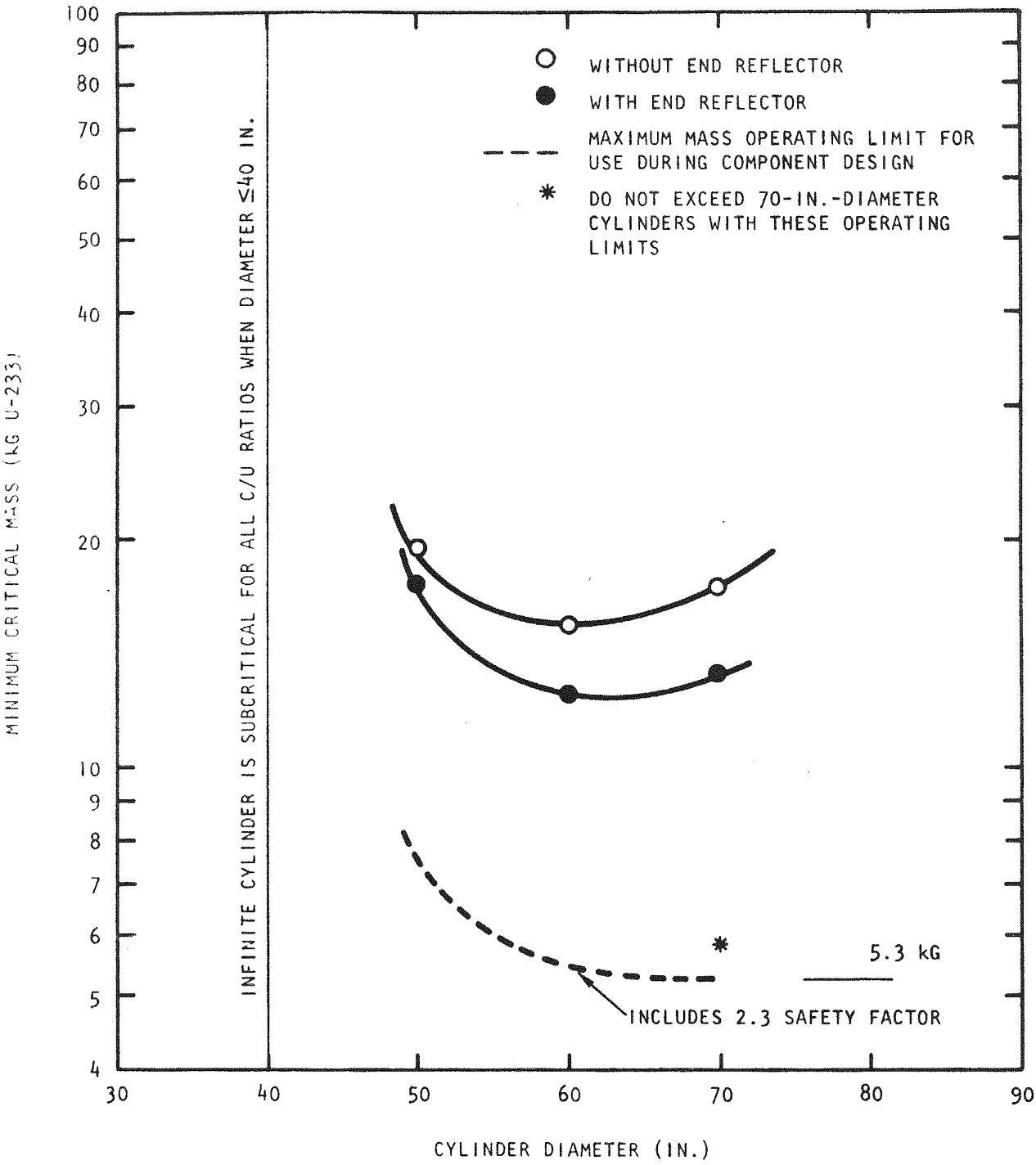

Fig. 5.7. Critical mass versus cylinder diameter, graphite moderated, Th/U = 10

less than 1 kg of U-233. If a design can be perfected that ensures water flooding is impossible, the allowable mass and diameter limits can be considerably increased.

In the commercial reprocessing plant, 150 fuel elements/day would be burned in eight burners, each 24 in. in diameter. The residue, if no product were removed, would contain 6 kg U-233 and 2 kg U-235, a total of 8 kg. This is less than the allowable weight shown in Fig. 5.5. Under these circumstances, 24-in.-diameter burners are permissable.

HEAD-END REPROCESSING

Summary

The support structure for the full-scale crushing system has been designed. Testing and assembly of the full-scale crushing components are proceeding on schedule.

A series of experiments and an engineering analysis of hopper/auger systems are nearing completion. The results show promise in defining hopper/auger design parameters.

Burning operations have centered on the 10-cm primary (exothormic) burner to gather data for ICPP and to develop operating techniques with distributor plates. The formation of agglomerates, which has occurred during these operations, is being studied. The addition of a distributor plate to the small 10-cm primary burner has as yet shown no operating advantages.

The initial construction and shakedown phases have been completed for the leaching systems. Operations with unirradiated product ash [from the secondary (endothermic) burner] and thorex will begin in the near future.

Crushing and Solids Handling

Design of the structure that supports the three crushers in the full-scale crusher system has been completed.

Modification of the primary crusher is continuing and several components have been assembled.

The results of preliminary crushing tests of the secondary crusher are shown in Fig. 5.8. The curves show gradation of crushed product for various discharge gap widths or closed side settings. The manufacturer's estimated gradation curve is not for a specific material, but rather is based on a wide range of materials and feed sizes. The discrepancies between H-327 data and the manufacturer's data reflect the inability of the low-amplitude vibrating screen separator to compensate for the anisotropy of the graphite.

The engineering analysis of hopper/auger systems has been tested with experimental data, and the performance of a new hopper/auger system is encouraging. The new system, which is readily adaptable to the 20-cm primary (exothermic) burner exhibits stable volumetric flow rates and maintains a plane level (i.e., at right angles to the hopper axis) of feed material.

Burning

Primary (Exothermic) Fluidized Bed Burner Development

During the past quarter the primary burner development program has concentrated on the 10-cm burner. This program is aimed at obtaining processing and design information for ICPP. Present efforts are aimed at developing an operating technique with a distributor plate.

20-cm Primary (Exothermic) Fluidized Bed Burner

The 20-cm primary burner was not operated during the past quarter. It is planned that this burner will be modified to include a new feed and product system, incorporating a new auger designed from information gained in the hopper/auger study. Also, the product removal and support system that has been successfully tested on the 10-cm burner will be added. This

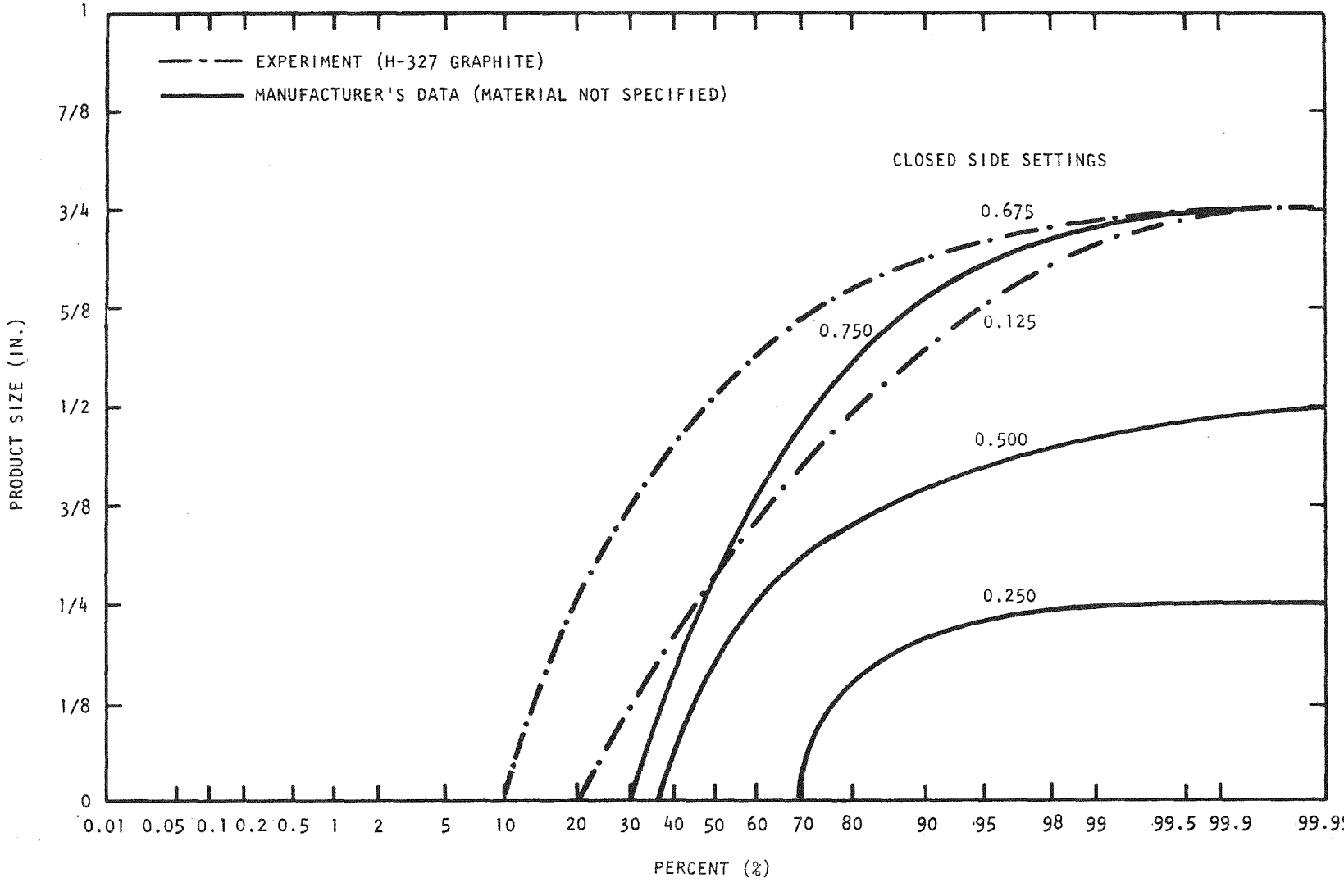

Fig. 5.8. Less than cumulative product gradation curve for secondary crusher

burner will not be modified to use a distributor plate until the distributor plate is evaluated on the 10-cm burner.

10-cm Primary (Exothermic) Fluidized Bed Burner

Seven runs were made in the 10-cm primary burner during the past quarter. These runs were all made with a distributor plate as part of a program to evaluate burner operation with a distributor plate. Only four of these runs were successful. The other three runs, and two ignition tests, resulted in aborted runs due to hot spots and poor operation.

Table 5.1 summarizes the runs made in the 10-cm primary burner using the present burner configuration. Runs 2, 3, and 4 were made without a distributor plate; the others were made with a distributor plate. No major modifications of the burner have been made in this series of runs (F4B-M) other than the addition of the distributor plate. Minor modifications have been made to improve burner-auger alignment, including a mechanism that constrains the burner to pure vertical motion when undergoing thermal expansion and the use of thin metal bellows with a metal sleeve for the product removal leg. These modifications have prevented deformation of the gas distributor and binding of the auger. The burner has also been modified to allow measurement of the fines carryover rate.

The distributor plate is being evaluated from several standpoints: (1) quality of fluidization (defined as a more even temperature profile), (2) fines carryover rate, (3) particle breakage, and (4) burner operability. During testing of the present distributor, shown in Fig. 5.9, only three successful runs have been made out of nine attempts. Successful runs were achieved only when the distributor plate had been removed and cleaned. Analysis of the bed and distributor plate after aborted runs revealed the presence of agglomerates, reaching the size of 6 cm by 4 cm by 3 cm and weighing up to 300 g. Run 10B was terminated after an agglomerate plugged

TABLE 5.1
PRIMARY BURNER RUN SUMMARY[a]

	F4B-M3[b]	F4B-M4[b]	F4B-M6	F4B-M7	F4B-M11
Burn rate (g/cm^2-min)	0.49	0.44	0.84	0.66	0.64
Superficial velocity (cm/sec)	89	75	104	77	102
Bed size per unit area (g/cm^2)	56	89	43	63	50
Bed temperature (°C)	972	970	965	965	950
Oxygen concentration (%)	84	86	87	81	82
Bed average particle size (μm)	640	860	600	600	560
Fines carryover rate (g/g burned)	--	--	0.16	0.04	0.03

[a] Runs 5, 8, 9, 10a, 10b, and 12 were aborted due to agglomerates.

[b] Did not have a distributor plate.

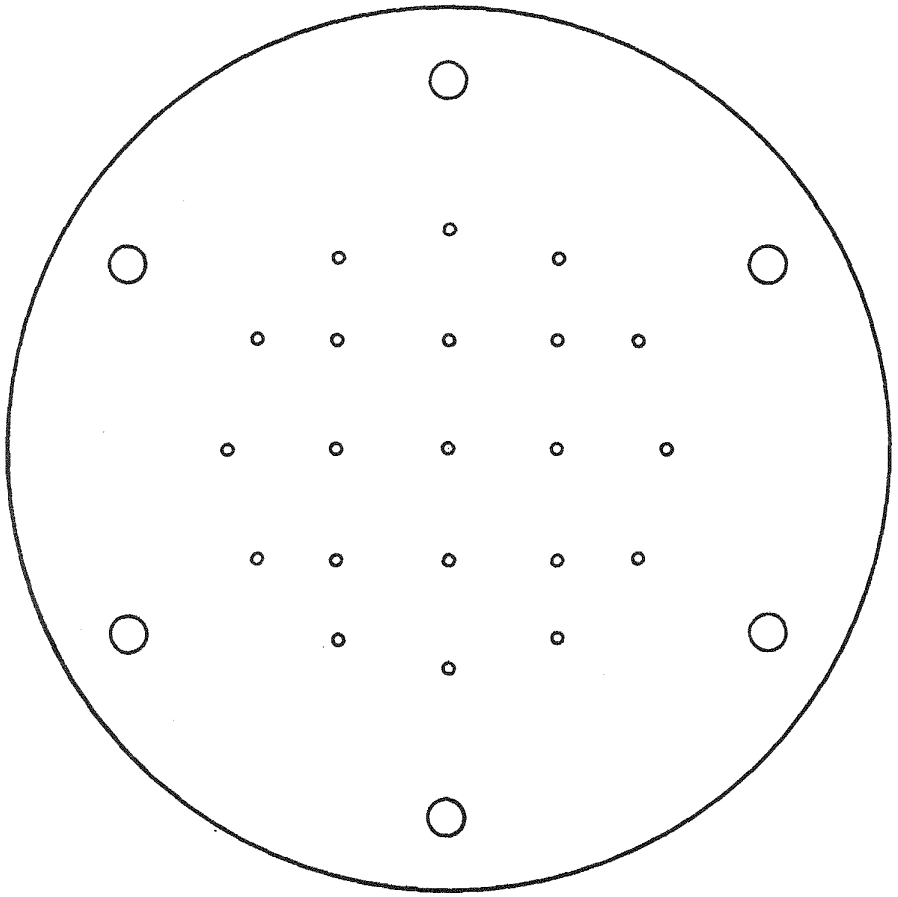

PLATE: 6-IN. DIAMETER, 304 STAINLESS STEEL, 1/4 IN. THICK

DISTRIBUTOR PATTERN: 21 1/16-IN. HOLES (12 EQUALLY SPACED ON 3-IN.-DIAMETER CIRCLE AND 9 IN A SQUARE PATTERN

FLANGE HOLES: 6 1/4-IN. HOLES EQUALLY SPACED ON 5-IN. DIAMETER

Fig. 5.9. Distributor plate

and bound the feed auger. The agglomerates form around the jet leaving the distributor plate orifices. Agglomerates have been found which range in size from small "droplets" of ThO_2 ($\sim$1 cm in diameter) to the larger chunks; it appears that the larger chunks grew from the smaller droplets. These agglomerates apparently grew up from the plate around the orifices, with the larger chunks having a hole through them where the gas blew through. Some of the distributor orifices also plug when agglomeration occurs. During runs where these agglomerates form, local "hot spots" were observed on the burner walls, and temperature control was difficult.

Further tests will be made to determine the cause of the agglomeration problem. Presently the use of the distributor has necessitated cleaning the plate for every successful startup. The local hot spots and agglomerate formation do not suggest an improved quality of fluidization. Figure 5.10 shows the temperature profiles for run F4B-M3 (4.5-kg bed) and run F4B-M11 (4.1-kg bed). Based on these data, the distributor plate has not resulted in an improvement in the temperature profile.

The measured fines carryover rate is shown in Table 5.1. The rate measured in the 20-cm burner without a distributor plate was $\sim$0.2 g fines/g graphite burned. The large discrepancy in the data for the 10-cm burner may be due to the measuring technique. During run F4B-M11 large temperature and CO percentage variations occurred periodically, probably resulting from fines agglomerating in the heat exchanger and falling back into the bed.

Increased attention is being paid to particle breakage. Several tests have been made to determine the fraction of broken particles in the burner and augers. An attrition test was made by fluidizing a bed of particles with a distributor plate; this test was made with air, no combustion, and adjustment of flow to give the same fluidizing conditions ($U - U_{mf}$) present in a run. The resulting breakage was 0.4% for 7 hr, which corresponds to

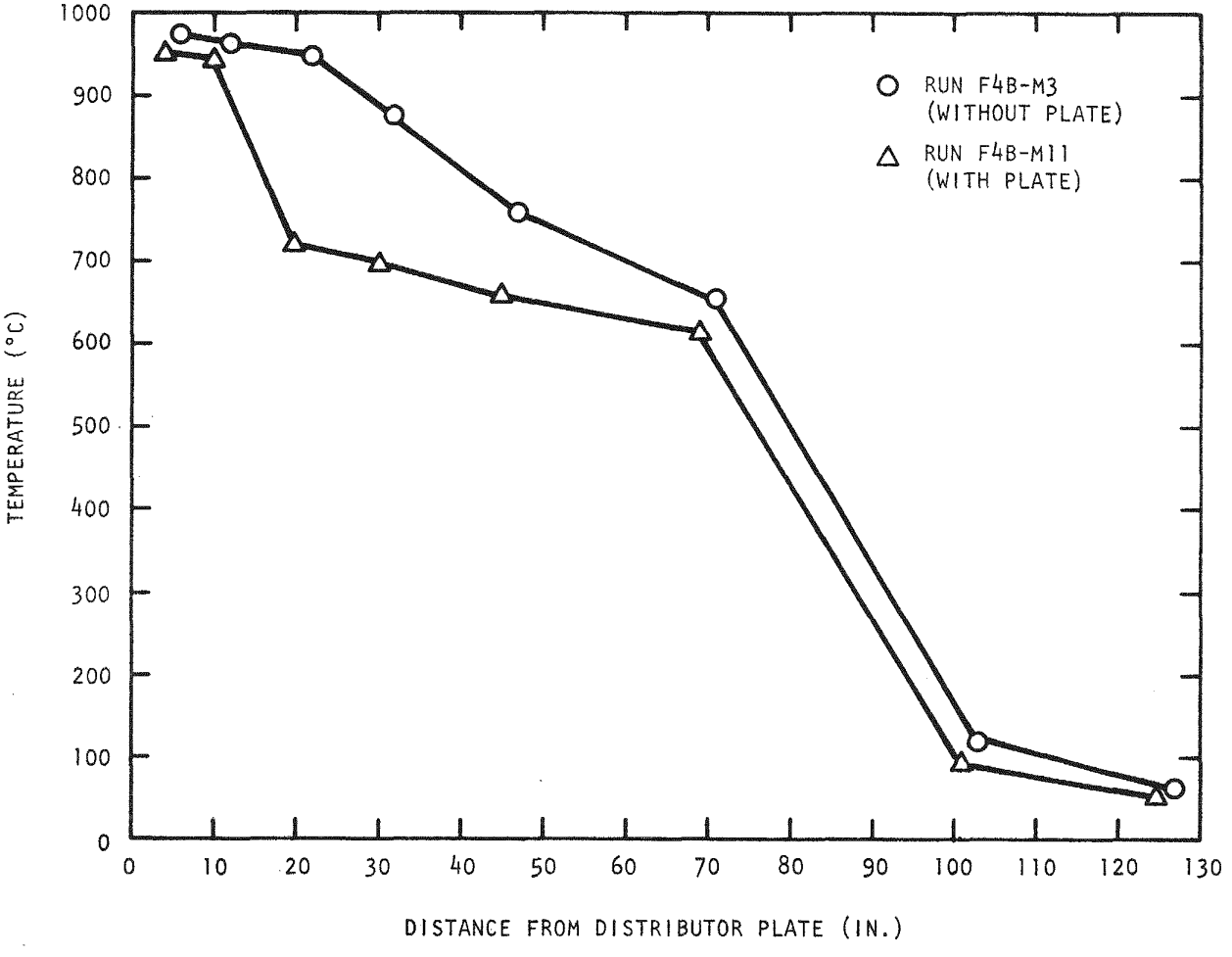

Fig. 5.10. Temperature profile with and without distributor plate

the residence time of a particle and one bed changeover. Run F4B-M6 was made with all graphite feed and a bed of particles; the run operated for 7 hr and resulted in 10% broken particles. The bed addition auger caused 6% of this breakage, indicating that about 4% broke in the bed during combustion. Runs F4B-M7 and F4B-M11 lasted 7 hr, one bed changeover, and resulted in 14% and 15% broken particles, respectively. The feed for these runs contained ∿3% broken particles; assuming 4% of the particles broke in the bed, the feed and product augers broke about 8% of the particles. Separate particle breakage tests are being made on ship's augers, similar to those used to feed the 10-cm primary burner, and for conventional core-type augers. The feed augers will be changed to an improved design based on the results of the recent auger study. The new system should have several advantages: (1) improved process seal, (2) smoother discharge and a more sensitive controller response, and (3) lower particle breakage.

Table 5.2 gives a more detailed analysis of data obtained from run F4B-M11. Product 8 was the last product cut, taken in the seventh hour of operation, from the burner. It appears that the burner had nearly reached steady-state operation at this time; the percentages of broken particles in the product and in the bed had reached the same level, and the carbon content in the product remained about constant throughout the run. The fines are mostly carbon. A longer term run will be made to determine if ThO_2 fines build up in the recycle stream.

TABLE 5.2
RUN F4B-M11, BED AND PRODUCT ANALYSIS

	Final Bed	Product 8	Product 7	Product 4	Fines
Burnable carbon (%)	5.2	9.0	11.0	9.9	86.7
Average particle size (μm)	560	560	520	--	<44
Broken particles (%)[(a)]	15.2	15.8	3.4	--	100

[(a)] Percent of material -420 μm after burning off all carbon.

10-cm Secondary (Endothermic) Fluidized Bed Burner

The 10-cm secondary burner was operated for eight runs during the quarter. The burner was modified by the addition of a clamshell cooler to the midsection. This modification allows high burn rates while maintaining lower filter temperatures. Table 5.3 summarizes the runs made during the quarter. Runs F4RHB-M13, -M14, -M16, and -M18 were made with the resistance heater removed during most of the run, allowing higher heat transfer from the bed and a faster burn rate.

Runs F4RHB-M16 and F4RHB-M17 were made with finely ground material having an average particle size of 55 μm. Both runs experienced hot spots indicative of poor fluidization. Temperature control was difficult for both runs. The product from run F4RHB-M16 had an unacceptably high carbon content, 16%, compared with the "normal" product, <2%, when burning 200-μm feed. The presence of 20% fertile inerts in run F4RHB-M17 did not improve operation and this run was shut down. It was concluded that material ground to ∿60 μm is not desirable as feed for the secondary burner.

Runs F4RHB-M12, -M13, -M14, -M15, -M18, and -M19 were made with nominal 200-μm feed and were shut down at the "crossover" point. This is the point in the run where the off-gas CO_2 level drops and the O_2 level rises until the measured concentrations cross over. The concentrations change very rapidly when the run is over, followed by a slow drop in temperature. This shutdown condition has reliably produced <2% burnable carbon in the product and usually produces <1% product.

Run F4RHB-M19 was made with a distributor plate. This run was routine and demonstrated the operability of the secondary burner with a distributor without an inert bed. The run exhibited no hot spots and no agglomerates. The success of this run apparently eliminates exposed ThC_2 kernels from broken particles as the source of the agglomeration problem in the 10-cm primary burner. The use of a distributor plate did not have any noticeable

TABLE 5.3
SECONDARY BURNER RUNS

	F4RHB -M12	F4RHB -M13	F4RHB -M14	F4RHB -M15	F4RHB -M16	F4RHB -M17	F4RHB -M18	F4RHB -M19
Feed (% burnable carbon)	17	15	11	11	18		15	14
Feed, particle diameter (μm)	190	200	260	210	55	55	250	200
Burn Conditions								
Temperature (°C)	1000	980	960	1025	775		940	950
Flow (liters/min STP)	110	140	114	50	64		105	130
O_2, average (%)	46	80	86	55	71		82	52
Burn rate (g C[(a)]/min)	24.4	56.0	46.7	13.7	24.3		42.7	27.2
Product (% burnable carbon)	1.8	0.2	1.0	0.3	16.7		0.3	0
Product, particle diameter (μm)	64	48	120	67	<44		66	56
Shutdown conditions (% CO_2/% O_2 outlet)	33/61	8/62	4/65	8/64	25/65		50/50	6/36

[(a)]Based on carbon equivalents; includes oxidized ThC_2.

effect on burner operation. The burn rate and temperature profile remained the same when using a distributor plate (see Fig. 5.11). The use of a distributor plate will necessitate modification of the secondary burner to allow remote dumping. At present the plate must be mechanically removed from the burner, allowing the finely ground material to escape and resulting in a product loss. Several alternative designs are being considered to allow remote dumping with product containment.

Leaching Systems

A leaching system has been constructed for operation at 10 to 20% of the expected capacity (see earlier Quarterly Progress Report, Gulf-GA-A12150) of the "hot demonstration" facility at ICPP. Basically, this system consists of (1) two air-sparged leachers that are operated as single batch or in a countercurrent series manner, (2) a batch centrifuge for centrifugal filtration or centrifugal sedimentation of solids from liquid phases, (3) steam-jet ejectors for transfer of liquids and slurries, and (4) sufficient auxiliary tankage for storage of reagents and products. This system is instrumented and will be operated on a remote basis from a central control room. All tankage is equipped with nitrogen purge systems and differential pressure transmitters to allow determination of liquid levels and specific gravities. These data are continuously recorded and will be used for material balance purposes.

Layouts of the 13-cm-diameter and 20-cm-diameter leaching vessels are given in Figs. 5.12 and 5.13, respectively. As shown in the figures, both vessels (1) are air-sparged, (2) have a bottom cone section, (3) are electrically heated, (4) utilize down draft condensers, and (5) have water cooling jackets. The centrifuge being utilized is a batch (30-cm diameter) basket centrifuge. A 1-hp dc variable speed motor allows a centrifuge operating range of 0 to 1550 g. The layout for a typical storage tank is shown in Fig. 5.14. These storage tanks have a capacity of about 45 liters.

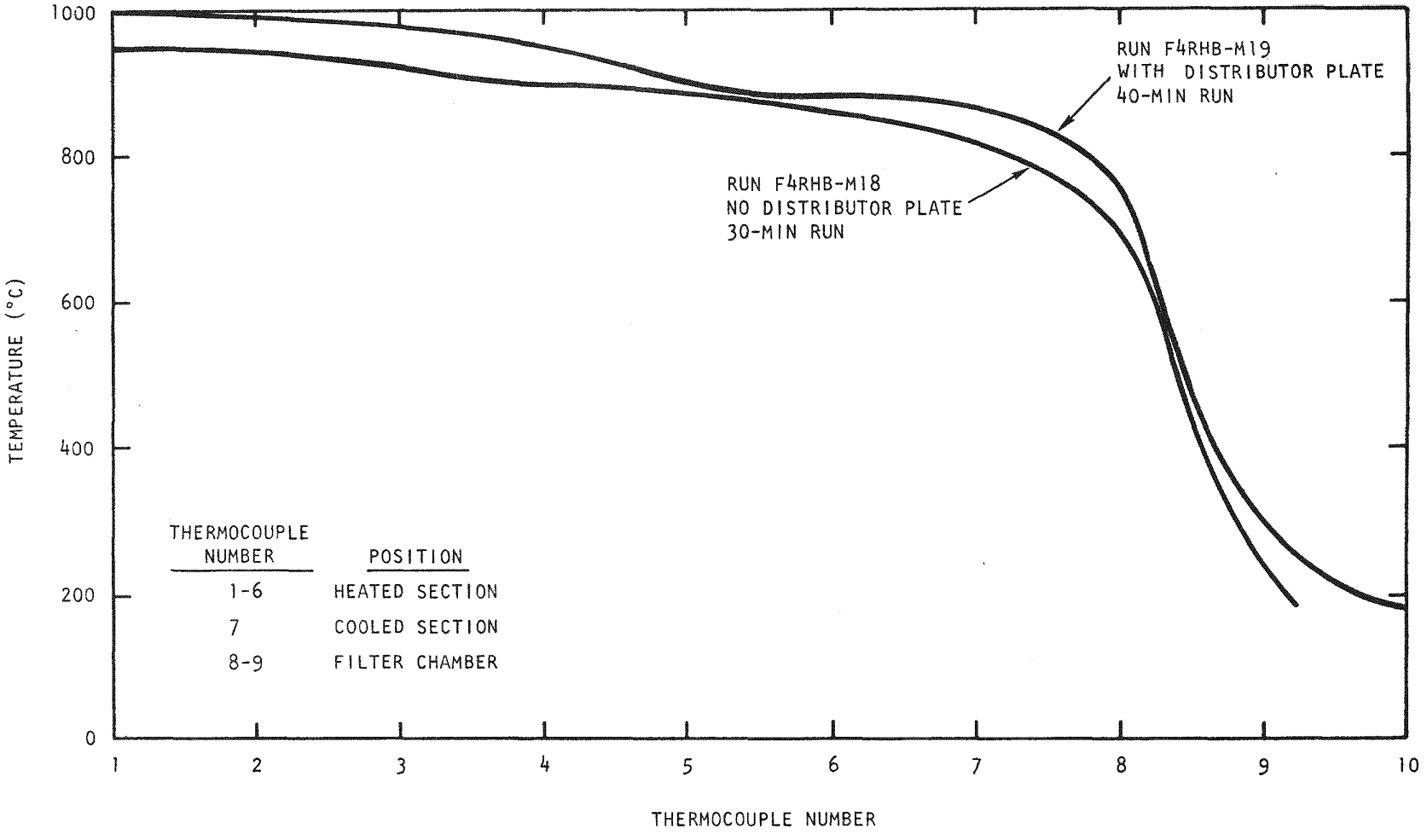

Fig. 5.11. Temperature profile by thermocouple number

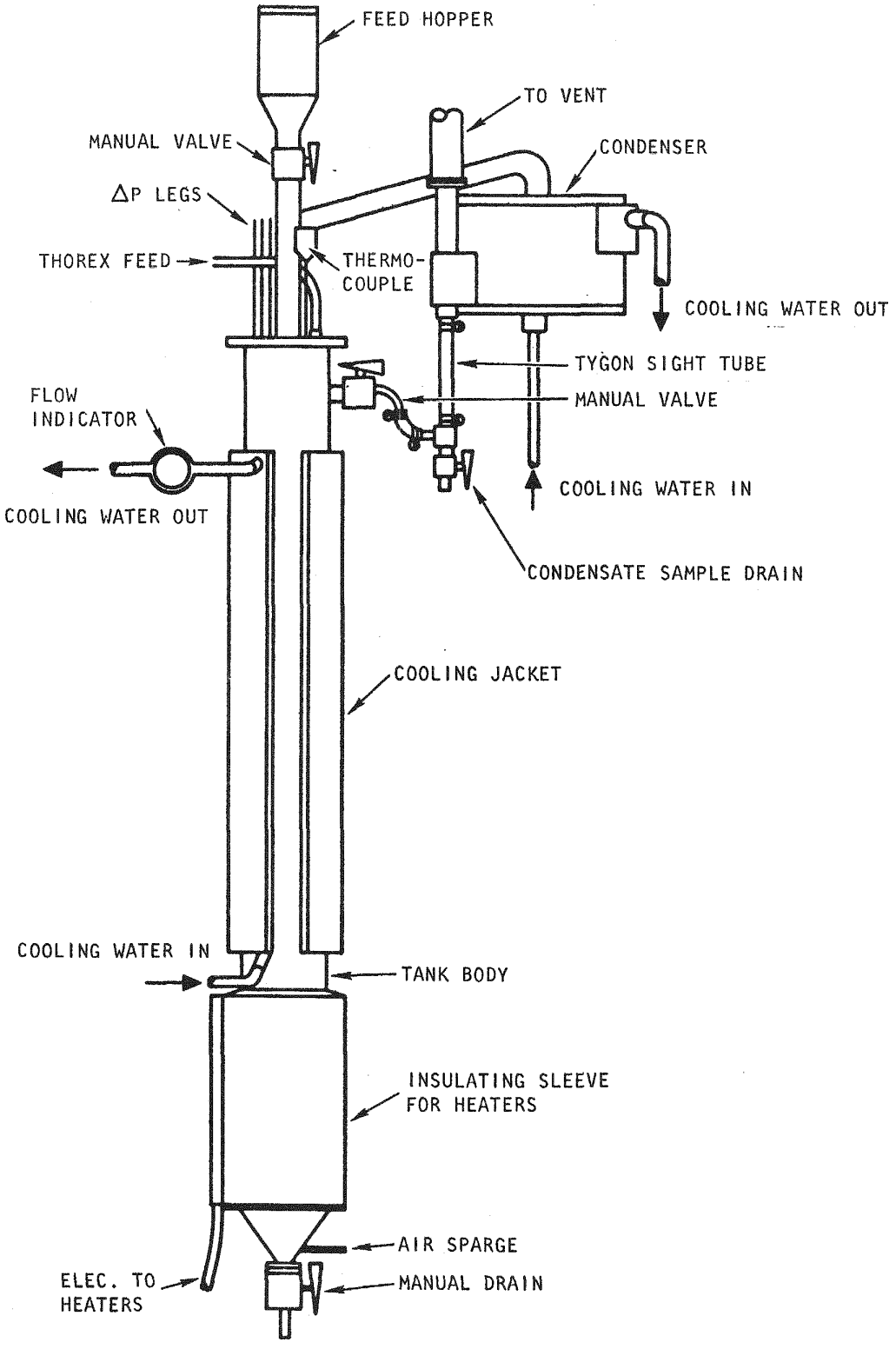

Fig. 5.12. 13-cm leacher

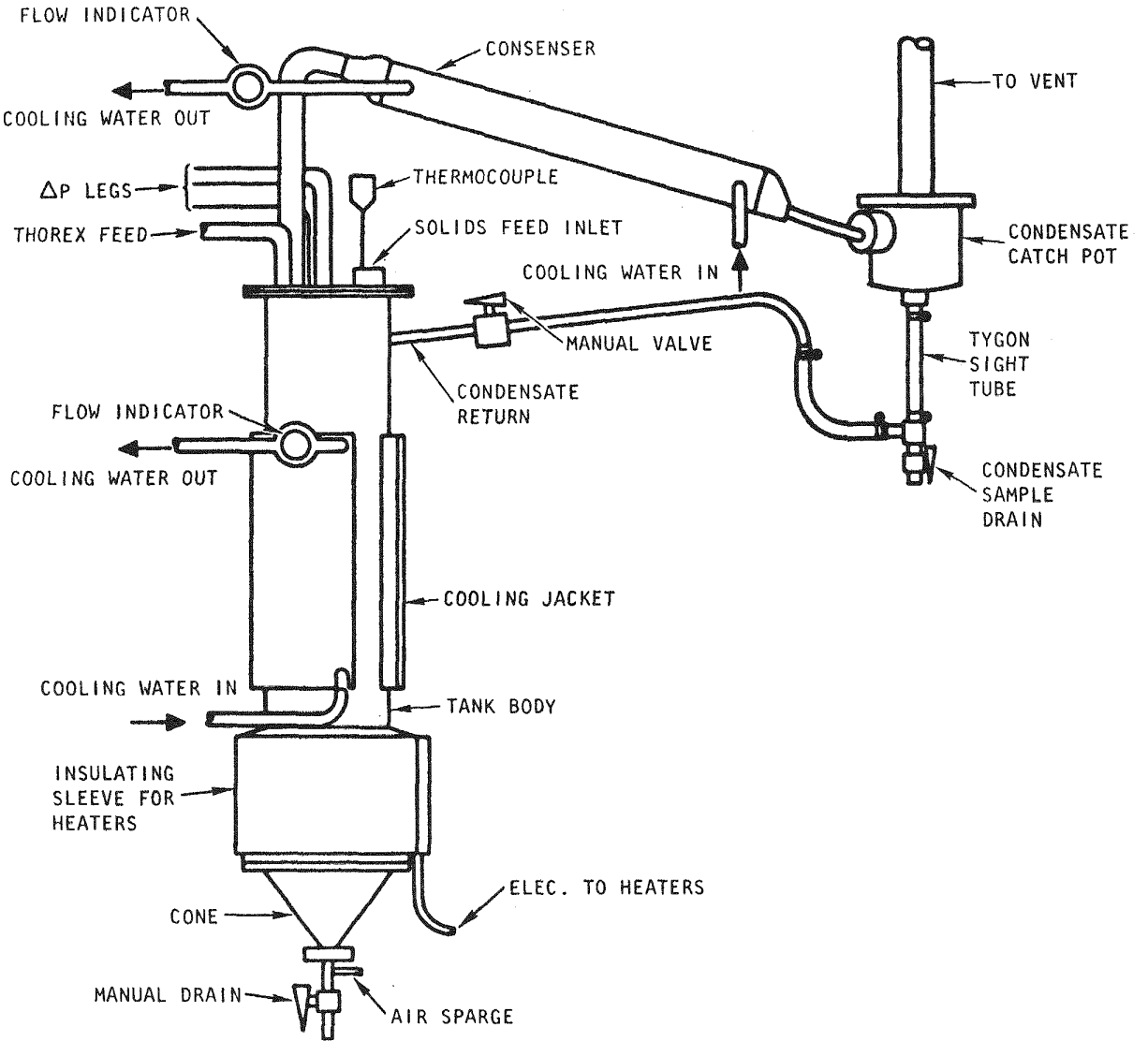

Fig. 5.13. 20-cm leacher

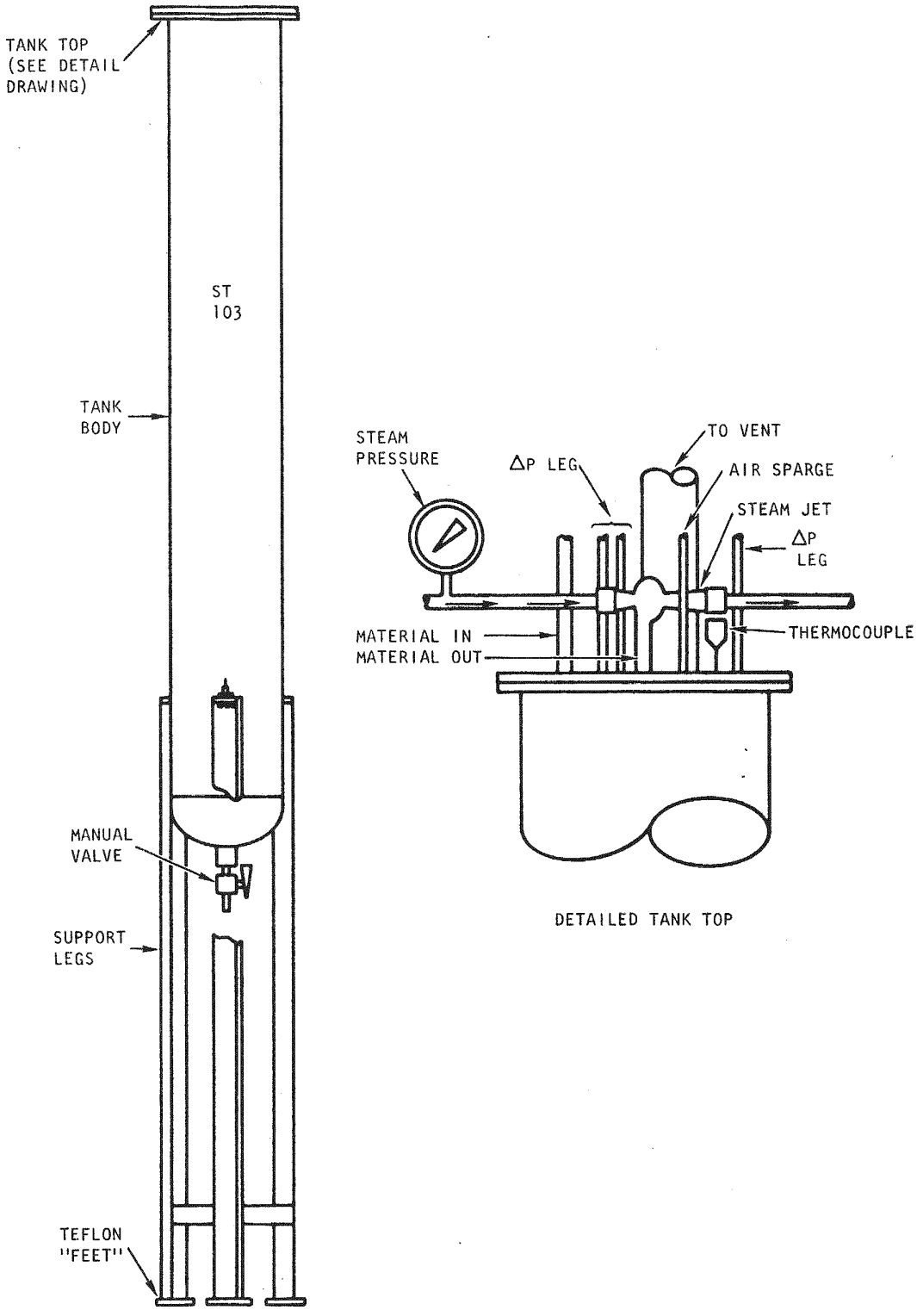

Fig. 5.14. Typical storage tank

The construction material for leachers, centrifuge, and storage tank is 304 L stainless steel. All of this process equipment is contained in a special "acid-proof" room to reduce the probability of contacting any other head-end reprocessing equipment with nitric acid. Also, off-gas from this system is scrubbed with water before venting to an absolute filter system.

The process has been leak-checked and has undergone shakedown with water. Calibration of instruments and tankage has been completed.

Planned additions to this system are (1) a solids dryer, (2) a solids classifier, and (3) a denitrator-evaporator.

REFERENCES

5.1. Wälti, P., and P. Koch, "A Two-Region Flux Spectrum Code for the Efficient Calculation of Group Cross Sections," Gulf General Atomic Report Gulf-GA-A10827, April 14, 1972.

5.2. Archibald, R., K. D. Lathrop, and D. Mathews,"1DFX, A Revised Version of the 1DF (DTF-IV) SN Transport Theory Code," Gulf General Atomic Report Gulf-GA-B10820, September 27, 1971.

TASK VIII
PHYSICS AND FUEL MANAGEMENT

CROSS SECTION EVALUATION WORKING GROUP (CSEWG)

Additional cross-section processing code benchmark calculations for the tedium isotopes were performed with the GFE2 code and will be forwarded to the CSEWG. A literature search for U-237, U-239, Am-241, and Am-243 cross-section data was initiated. If sufficient new data are available to justify the effort, it is planned to prepare updated versions of the ENDF/B data sets for these nuclei for submission to the CSEWG. The GAND2/GFE2 cross-section processing codes are being documented.

CRITICAL EXPERIMENT ANALYSIS

The ENDF/B Version II data for Pu-239 assumes that Doppler broadening effects are negligible below 1 eV, whereas older GGA evaluations predict some temperature dependence near 0.3 eV. By Doppler broadening the Version II data numerically, it was concluded that the capture-to-fission ratio is not significantly affected, but that the grain shielding might change slightly near 0.3 eV. A similar analysis was performed for U-233 and no significant temperature dependence was observed below 1 eV. No significant change in the computed temperature coefficients for the High-Temperature Lattice Test Reactor (HTLTR) Pu/Th lattice would result from such Doppler broadening effects.

Revised calculations for the first U-233/Th HTLTR lattice using the as-built atom densities showed a 0.004 (0.4%) increase in k_∞ at room temperature and an insignificant change in computed temperature defect as compared with the previously reported GGA calculations.

FAST NEUTRON DOSIMETRY

Work on fast neutron damage in connection with the irradiation test program continued. An ETR irradiation of graphite samples was re-analyzed and related to HTGR conditions on the basis of the relative numbers of displaced carbon atoms per unit neutron fluence. The displacement cross-section production function used in this work was the one recently recommended by an IAEA Working Group for use in reporting and correlating the results of such irradiation experiments.

FUEL TEST ELEMENTS

The final plans and procedures for the postirradiation examination of FTE-3 have been completed.

During a part of October and during all of November 1972, the Peach Bottom reactor was operated at a reduced (∿75%) power level, which also caused test elements FTE-4, -6, -14, and -15 to operate at a reduced power level. Full-power operation of the reactor was restricted by the necessity to maintain the concentration of methane in the main coolant at ≤2 ppm. On November 25, 1972, the reactor was shut down to remedy the oil ingress problem responsible for the hydrocarbon impurities. Repairs were completed and the reactor returned to power on January 10, 1973.

The reactor and test elements have operated at full power through January 1973 without incident.

Recycle Test Element Temperatures

An investigation of the predicted versus actual test element temperatures was completed during the quarter. Test elements (FTE-4, -6, -14, and -15) are instrumented with two thermocouples in the fuel body: a tungsten-rhenium thermocouple in the spine hole location and a chromel-alumel thermocouple located in the graphite. The hot junctions of the

thermocouples are typically located at the positions of maximum fuel temperature (68 to 75 in. from the bottom of an element). None of the recycle test elements (RTE-2, -5, -6, and -8 and FTE-11) are instrumented with thermocouples.

The W/W-Re thermocouples in the spine holes give the best indication of the in-core performance of the test element. Although these thermocouples do not give a direct reading of the maximum fuel temperatures, computations with the TAC-2D heat transfer code (Ref. 8.1) in the R-θ transverse plane have indicated that the expected difference between the temperature at the spine hole thermocouple location and the maximum fuel temperature should not be too great; moreover, this difference should be predictable and appropriate corrections can be applied. There are, however, several complicating factors that must be considered before predicting maximum temperatures from W/W-Re thermocouple readings.

First, the thermocouples used in the test elements are W-3% Re/W-25% Re alloy, whereas the thermocouples used in Core 1, and the associated temperature recorder, were of the W-5% Re/W-26% Re type. This temperature recorder is also used with the test elements being irradiated in Core 2. The calibration curves for the two thermocouple types are similar but not identical. Consequently, a correction must be applied to the indicated temperature recorder when used with the W-3% Re/W-25% Re thermocouples; the recorder temperature reads about 40°F high. Secondly, W/W-Re thermocouples decalibrate under irradiation because of transmutation effects. For purposes of temperature correction, the decalibration curve shown in Fig. 8.1 was used (Ref. 8.2). There is still some question as to whether the transmutation reaction responsible for decalibration is best correlated with fast or with thermal flux, but for the purposes of this study the thermal flux correlation was used.

When the above factors are taken into consideration, a fairly accurate determination of the temperature at the spine hole location is possible. As mentioned previously, there is a temperature drop from the maximum fuel temperature, which is the temperature that must be considered. At beginning-of-life, this temperature difference can be predicted with some confidence;

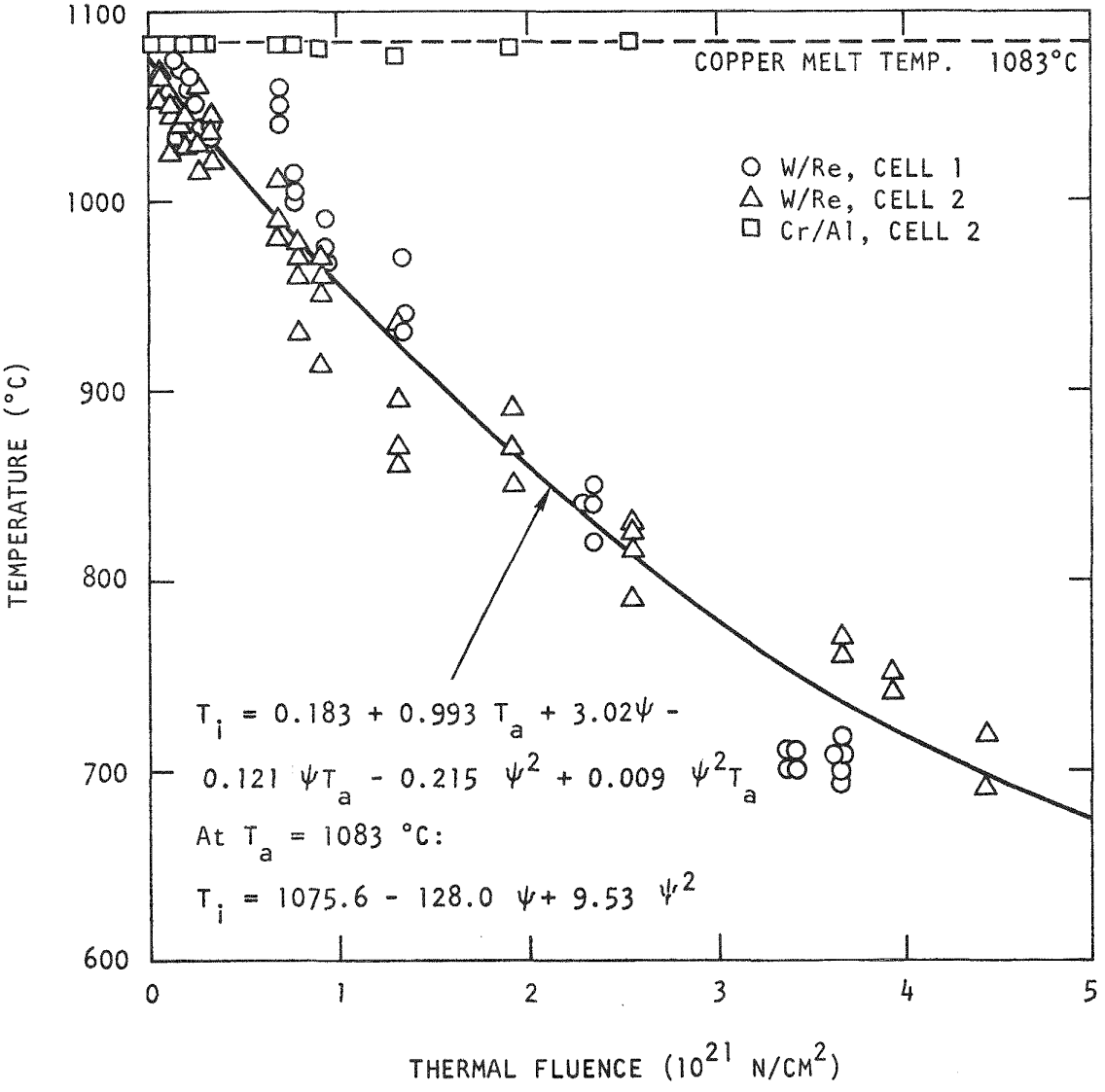

Fig. 8.1. Thermocouple calibration cell contained in irradiation capsule P13M, showing effect of neutron bombardment of emf output of W-3% Re/W-25% Re thermocouples by measuring melting point of copper

however, this difference is a function of graphite conductivity and of the fuel rod/fuel body gap, both of which change under irradiation. Typically, unirradiated needle-coke graphite has a thermal conductivity of about 25 Btu/hr-ft-°F at 1800°F; upon irradiation, the conductivity decreases to perhaps 16 Btu/hr-ft-°F at an exposure of about 3×10^{21} n/cm^2, after which the conductivity remains relatively constant to an exposure in excess of 10×10^{21} n/cm^2 (Refs. 8.3, 8.4). The fuel rod/fuel body gap tends to grow under irradiation as a consequence of nonuniform irradiation-induced dimensional changes.

Also, the fuel body/sleeve gap must be considered. Since the fuel body is free to move within the sleeve (nominal as-built clearance is 0.005 in.), a constantly changing eccentricity is expected; within the established limit (0.010 in.), this eccentricity could induce as much as 150°F oscillation in thermocouple readings.

Subject to the corrections and limitations described above, corrected thermocouple data were compared with predicted maximum fuel temperatures. The comparison was made for a time when the reactor and test elements were at full power. The selected time was at 400 EFPD of reactor operation. Two sets of thermocouple readings were selected from the weekly log sheets (July 14, 1972, and July 24, 1972) which bracket the 400 EFPD time step. The average readings of these two data sets are given in Table 8.1. These W/W-Re thermocouple readings were then corrected for the W/W-Re alloy difference and for transmutation using the thermal fluence correlation. Since the fast fluences for all the test elements were relatively low ($<2 \times 10^{21}$ n/cm^2), the effect of irradiation on graphite thermal conductivity and fuel rod/body gap was ignored as a first approximation.

TABLE 8.1
AVERAGE THERMOCOUPLE READINGS AT APPROXIMATELY 400 EFPD

Test Element	Average Uncorrected W/Re Thermocouple Reading (°F)	Average C/A Thermocouple Reading (°F)
FTE-4	1904	Failed
FTE-6	2238	1246
FTE-14	2290	Failed
FTE-15	1738	1389
FTE-11, RTE-2, RTE-5, RTE-6, RTE-8 (Not instrumented)		

Using power factors and reactor parameters that conformed reasonably with actual conditions, expected maximum fuel and graphite temperatures were predicted with the TAC-2D and TES heat transfer codes (Refs. 8.1, 8.5). The results of these computations are shown in Table 8.2. The expected temperature difference between the W/W-Re thermocouple location and maximum fuel temperature was then predicted as a function of linear power and applied to the W/W-Re data (already corrected for alloy and irradiation effects). These corrected W/W-Re readings and the uncorrected C/A readings are also indicated in Table 8.2 whenever available.

The chromel-alumel (C/A) thermocouples give a measure of the average graphite temperature. Since C/A thermocouples do not degrade under neutron bombardment, no decalibration correction need be applied to the readings.

Comparison of the predicted temperatures with the thermocouple data indicates that for all test elements, in general, the predicted maximum fuel temperatures and the properly corrected W/W-Re thermocouple readings

TABLE 8.2
COMPARISON OF CORRECTED THERMOCOUPLE READINGS VERSUS CALCULATED TEMPERATURES AT THE THERMOCOUPLE LOCATIONS

Test Element	Corrected W/Re Thermocouple Reading (°F)	Calculated Fuel Temperature at W/Re Thermocouple Location (°F)	C/A Thermocouple Reading (°F)	Calculated Graphite Temperature at C/A Thermocouple Location (°F)
FTE-4	2199	2100	Failed	1670
FTE-6	2553	2210	1246	1775
FTE-14	2425	2340	Failed	2000
FTE-15	1873	2340	1389	2000
FTE-11	Not instrumented	2330	Not instrumented	1830
RTE-2	Not instrumented	2020	Not instrumented	1665
RTE-5	Not instrumented	1980	Not instrumented	1610
RTE-6	Not instrumented	2030	Not instrumented	1648
RTE-8	Not instrumented	2000	Not instrumented	1602

are in good agreement. There are several notable exceptions, however, particularly test element FTE-15. According to repeated physics calculations using "as-built" loadings, the power generated in test elements FTE-14 and -15 should be the same. While FTE-14 is performing as expected, FTE-15 is running considerably cooler than anticipated. This anomaly has not yet been resolved and will continue to receive close attention. Inspection of the C/A thermocouple data, on the other hand, reveals only marginal agreement between expected and observed graphite temperatures. These discrepancies will also receive further attention. It is suggested that a number of the C/A thermocouples have actually failed and are simply giving erroneous readings.

The agreement between predicted and observed test element temperatures is reasonably good considering the number of variables involved. As additional information regarding irradiation-induced dimensional changes and thermal conductivity changes becomes available, more accurate predictions of test element temperatures will be possible. At present, predictions to within ±100°F should be considered excellent.

Beginning-Of-Life Linear Power

Beginning-of-life linear powers are reported for all test elements for comparison with those for Fort St. Vrain and large HTGR fuel elements.

Table 8.3 summarizes the average and peak beginning-of-life linear powers for all test elements. Linear power (in watts per centimeter) was computed for both the overall element and the individual fuel holes (i.e., per fuel rod or fuel bed). For eight-hole telephone dial elements, the average linear power ranged from 456 to 564 W/cm with corresponding peak values of 591 to 724 W/cm; on a per fuel hole basis, these values translate to 57.0 to 70.5 W/cm/hole and 73.9 to 90.5 W/cm/hole, respectively. The two six-hole telephone dial elements (FTE-14 and -15) have identical linear

TABLE 8.3
BEGINNING-OF-LIFE LINEAR POWER OF PEACH BOTTOM FUEL TEST ELEMENTS
AT 95% POWER

Phase	Test Element	Bed Type	Beginning-of-Life Linear Power			
			Per Element[a]		Per Fuel Hole[b]	
			Average (W/cm)	Peak (W/cm)	Average (W/cm/zone)	Peak (W/cm/zone)
1	RTE-2	Mixed (3B,3R)[c]	456	591	57.0	73.9
1	RTE-4	Mixed (3B,3R)	509	654	63.6	81.8
1	RTE-5	Rods	490	630	61.2	78.8
1	RTE-6	Rods	503	646	62.9	80.8
1	RTE-7	Rods	466	598	58.2	74.8
1	RTE-8	Mixed (1B,5R)	521	669	65.1	83.6
2	FTE-11	Rods	656	843	82.0	105.3
2	FTE-4	Rods	558	717	69.8	89.6
2	FTE-6	Rods	564	724	70.5	90.5
3	FTE-14[d]	Rods	496	638	82.7	106.3
3	FTE-15[d]	Rods	496	638	82.7	106.3

[a] Power generated per centimeter of element.

[b] Power generated per centimeter of element per fuel rod (or fuel bed).

[c] B = blended bed (close-packed assembly of unbonded coated fuel particles).
R = rods (close-packed assembly of coated fuel particles bonded together with a carbonaceous matrix.

[d] Linear power at 16 EFPD exposure because of nontypical rod pattern at beginning-of-life.

powers of 496 W/cm average and 638 W/cm peak or 82.7 W/cm/hole average and 106.3 W/cm/hole peak. In comparison, Fort St. Vrain fuel elements have core average linear powers of 39.5 W/cm/rod and peak linear powers of 102.6 W/cm/rod at beginning-of-life; the large HTGR fuel elements have powers of 82 W/cm/rod average and 186 W/cm/rod peak.

The linear powers of Peach Bottom test elements were obtained from the TES code (Ref. 8.5). The TES code calculates power generation in an element by integrating the axial flux profile with appropriate radial power factors provided from physics calculations. Overall linear powers so obtained were then translated to a "per fuel hole" basis by simply dividing by the number of fuel holes.

A logical time reference for comparing linear powers of fuel elements is beginning-of-life. Consequently, for all Phase 1 and 2 test elements, the reported linear powers are beginning-of-life values. However, for Phase 3 elements (FTE-14 and -15), the beginning-of-life linear power values were untypically lower than design values. This discrepancy resulted from unfavorable control rod configuration at the time of insertion of Phase 3 elements (384 EFPD). Thus, for the above Phase 3 elements, the reported linear powers are not beginning-of-life values but reflect operation after short exposures, which correspond to control rod configurations considered more typical.

Fuel Test Element No. 19

The scope of work for Task VIII of the HTGR Base Program for FY-73 covers the design, fabrication, surveillance, and postirradiation examination of fuel test elements. Among these fuel test elements, FTE-19 was to be inserted in the Peach Bottom Reactor for testing HTGR fuels at high temperatures for 300 EFPD. The element was to be inserted in the reactor at the last scheduled fuel handling shutdown before the end-of-life of Core 2. This shutdown has been scheduled to begin on April 1, 1973, which would require completion and acceptance of FTE-19 fuel rods by March 1, 1973.

It became apparent during the quarter that the original amount of fuel needed for FTE-19 could not be delivered on time due to the priority in fabricating fuel for capsule P13Q. An attempt was made to redesign FTE-19 using a new fuel body arrangement that would greatly reduce the quantity of fuel rod required (to ~150 in.). It was originally anticipated that the objectives for FTE-19 could be achieved with this design and, in addition, the redesigned test element would serve as a severe stress test within one of the graphite fuel bodies. Analytical studies, however, established that this concept would not perform as desired. As a result, FTE-19 has been deleted from the fuel element test program.

The objective of FTE-19 was to test large HTGR fuel at high temperatures for a relatively short period of time to investigate fuel operating limits at high temperatures. The maximum fuel design temperatures were to be on the order of 2550° to 2650°F. In the center fuel body of Phase 3 test elements FTE-14 and FTE-15 predicted temperatures up to 2700°F will be achieved. This will give, in part, some of the same information expected from PTE-19.

REFERENCES

8.1. Clark, S. S., and J. F. Petersen, "TAC-2D, A General Purpose Two-Dimensional Heat Transfer Computer Code," USAEC Report GA-9262, Gulf General Atomic, September 1967.

8.2. Carpenter, F. D., N. L. Sandefur, R. J. Grenda, and J. S. Steibel, "EMF Stability of Chromel/Alumel and Tungsten-3% Rhenium/Tungsten-25% Rhenium Sheathed Thermocouples in a Neutron Environment," Gulf General Atomic Report GA-10384, October 1, 1970.

8.3. Engle, G. B., and A. L. Pitner, "High-Temperature Irradiation Behavior of Production-Grade Nuclear Graphites," USAEC Report GA-9973, Gulf General Atomic, July 10, 1970.

8.4. Engle, G. B., and K. Koyama, "Thermal Conductivity Changes in Nuclear Graphites at High Temperatures and High Fluences," USAEC Report Gulf-GA-A12137, Gulf General Atomic, June 30, 1972.

8.5. Vrouwes, J. H. L., and D. L. Hanson, "Thermal Analysis of Fuel Test Elements," Gulf General Atomic Report Gulf-GA-A10911, to be published.

TASK IX

FUELS MATERIALS DEVELOPMENT

FUEL IRRADIATIONS

A series of capsule irradiations is being conducted to evaluate recyclable fuel systems for a large HTGR under the irradiation environments expected in a large HTGR.

Capsules P13N and P13P

Capsules P13N and P13P are companion tests and are the fourth and fifth in a series of irradiation tests of candidate HTGR recyclable-type fuels. These capsules are the first P-capsules being monitored for in-pile fission gas release during irradiation. Each capsule contains five cells in which both fuel rod and unbonded particle samples are being tested; oxide and carbide fuels are included. Irradiation exposures of P13N and P13P are designed to span a wide range of conditions in an effort to define operating limits for these fuels. Capsule P13N was designed for peak irradiation up to $\sim 6 \times 10^{21}$ n/cm^2 (E > 0.18 MeV) at 1350° and 1500°C. Capsule P13P is designed for irradiation at 1050° and 1350°C to peak exposures of $\geq 8 \times 10^{21}$ n/cm^2.

Capsule P13N completed its scheduled irradiation during this reporting period. It was discharged from the ETR on January 5, 1973 and has been sent to the GGA Hot Cell facility. It is estimated to have reached a peak fast fluence of 5 to 6 x 10^{21} n/cm^2. Postirradiation examination of this capsule is scheduled in the near future.

Capsule P13P is continuing its irradiation in the ETR. However, because of past and projected extended downtimes of the ETR, the expected

exposures for this experiment may be significantly reduced from the original design values. Capsule P13P has reached an estimated peak exposure of 5.4×10^{21} n/cm^2. The unbonded particle beds continue to operate 100° to 400°C hotter than design in most of the cells; however, fuel rod samples have been operating very close to their design temperatures. Fission gas release values continue to be obtained from each of the five separate cells. These data indicate that the three cells operating at ∿1350°C have Kr-85m fractional R/B values of 5×10^{-4}; the two cells operating at ∿1050°C have fractional R/B values in the range of 2×10^{-5}. Particles are designed to fail in the 1350°C cells at these exposures and, in part, are believed to be the cause for the higher gaseous release from these cells.

Capsules P13R and P13S

The initial thermal design studies for the P13R and P13S capsules have been completed. Analyses of the results from this work are in progress and recommendations for the final thermal design will be made. This work is expected to be completed during the next quarter.

GGA-ORNL Cooperative Irradiation Capsules

A series of cooperative irradiation tests are being carried out with ORNL in their irradiation facilities. These irradiations include tests in the HFIR target position (HT-capsules), the HFIR beryllium-reflector position (HRB-capsules), and the ORR facility.

Capsule P13Q

Fuel particle fabrication for P13Q was completed. There are currently three batches of BISO coated ThO_2 and one batch of TRISO coated UC_2 available for use in the experiment. In addition, two batches of BISO coated, carbon kernel inert particles were fabricated. Thermal design of capsule P13Q, including both beginning-of-life and end-of-life conditions, was also completed. Following completion of the thermal design, fuel rod fabrication was initiated and is currently in progress.

Capsules HRB-4 and HRB-5

Capsules HRB-4 and HRB-5 are two of the most recent capsules in a series of tests being irradiated in the ORNL HFIR. These two experiments are sponsored by ORNL but represent a cooperative GGA-ORNL irradiation effort designed to evaluate the irradiation performance of fuel rods that were fabricated using candidate processes and materials for large HTGR startup and recycle fuel systems. Both capsules were inserted in the beryllium-reflector position of the HFIR on October 8, 1972. Capsule HRB-4 is scheduled to be irradiated to a peak fluence of $\sim 8 \times 10^{21}$ n/cm^2 (11 cycles), while capsule HRB-5 is scheduled for irradiation to $\sim 3.6 \times 10^{21}$ n/cm^2 (5 cycles). The design temperatures for both capsules are 900° and 1200°C, and both capsules are being monitored for in-pile fission gas release during irradiation.

The GGA portions of each capsule contain two each of three different types of fuel rods (a total of 12 rods in the two capsules). These samples include rods fabricated with three different graphite fillers, one binder, and two types of graphite shim material. All the rods were fabricated by the admix-compaction process and were carbonized and high-fired in H-327 graphite tubes to simulate in-block curing. A description of the fuel rods being irradiated in capsules HRB-4 and HRB-5 is given in the previous Quarterly Progress Report (Gulf-GA-A12422).

Capsule HRB-5 has been discharged from the beryllium-reflector region of the reactor after completing its scheduled five cycles of irradiation. It will remain in the reactor pool during an additional cycle for a calibration check of the acoustic thermometer in the capsule. Capsule HRB-4 will remain in the HFIR reactor for an additional five to six cycles as scheduled.

Fission gas release has been monitored in both capsules. The most recent reported Kr-85m R/B values were $\sim 6 \times 10^{-5}$ for HRB-4 and $\sim 5 \times 10^{-5}$ for HRB-5.

HRB-6

The purpose of the HRB-6 experiment is to evaluate the irradiation performance of fuel rods fabricated by both ORNL and GGA using candidate processes and materials for large HTGR startup and recycle fuel systems. The six GGA fuel rods to be included in this experiment were fabricated using the hot injection process and were cured in-place in H-451 graphite. HRB-6 is a companion capsule to capsules HRB-4 and -5 for which the admix compaction process was used, by GGA, to fabricate fuel rods that were then cured in-place in H-327 graphite. HRB-6 is scheduled for insertion in the beryllium-reflector position of the ORNL HFIR reactor in early March. The capsule is expected to operate at 1200°C to a peak fast neutron fluence of 9×10^{21} n/cm^2 ($E \geq 0.18$ MeV).

The matrix materials and particle loadings used in HRB-6 fuel rod fabrication are given in Table 9.1. The heavy metal requirements were supplied by ORNL. The fuel particles were coated at GGA and the inerts (BISO) were coated at ORNL. Details of the fuel rod matrix variables used in this experiment are also included in Table 9.1. This test will compare the irradiation behavior of hot injected rods whose matrices contain type 1089 isotropic graphite flour filler and type 1099 isotropic graphite powder shim (rods 7161-001-01-1 and -04-1) with rods containing type RC4 isotropic graphite filler and shim (7161-001-03-1 and -06-10). Also included are two rods with type 1089 isotropic graphite flour, 1099 shim, and 3% addition of a mold release additive. All matrices used type A240 petroleum pitch binder and each rod was cured at 1800°C in H-451 graphite.

Fabrication of these rods was completed in early January, and the rods were shipped to ORNL on January 15, 1973.

Capsules HT-12, HT-13, HT-14, and HT-15

The current HT series (HT-12, -13, -14, and -15) was designed to permit examination of the irradiation behavior of unbonded particle samples of

TABLE 9.1
COMPOSITION OF HOT-INJECTED, CURED-IN-PLACE FUEL COMPACTS FOR HRB-6/7 IRRADIATION EXPERIMENTS

Position in Capsule	Sample Number	Expected Fast Neutron Exposure (n/cm^2) (E>0.18 MeV)	Matrix Composition[a]		Particle Loading								U-235 Content (g)	U Content (g)	Th Content		
					Fissile[b]		Fertile[c]		Inert[d]		Shim						
			Filler	Shim	Weight (g)	Vol. (%)	Weight (g)	Vol. (%)	Wt. (g)	Vol. (%)	Weight (g)	Vol. (%)			Fissile (g)	Fertile (g)	Total (g)
2A	7161-001-01-1	9×10^{21}	Type 1089, isotropic graphite flour	Type 1099, isotropic graphite powder	0.2440	2.98	1.2397	12.66	1.00	22.17	1.0568	18.0	0.0161	0.0173	0.0620	0.6486	0.7106
2B	7161-001-02-1	9×10^{21}	Type 1089, isotropic graphite flour	Type 1099, isotropic graphite powder	0.2440	2.98	1.2397	12.66	1.05	23.27	1.0568	18.0	0.0161	0.0173	0.0620	0.6486	0.7106
2C	7161-001-03-1	9×10^{21}	Type RC4, isotropic graphite flour	Type RC4, isotropic graphite powder	0.2440	2.98	1.2397	12.66	1.00	22.17	1.0568	18.0	0.0161	0.0173	0.0620	0.6486	0.7106
4A	7161-001-04-1	6×10^{21}	Type 1089, isotropic graphite flour	Type 1099, isotropic graphite powder	0.2440	2.98	1.5794	16.12	0.86	18.94	1.0568	18.0	0.0161	0.0173	0.0620	0.8263	0.8883
4B	7161-001-05-1	6×10^{21}	Type 1089, isotropic graphite flour	Type 1099, isotropic graphite powder	0.2440	2.98	2.0891	21.33	0.63	13.96	1.0568	18.0	0.0161	0.0173	0.0620	1.0930	1.1550
4C	7161-001-06-10	6×10^{21}	Type RC4, isotropic graphite flour	Type RC4, isotropic graphite powder	0.2440	2.98	2.5982	26.52	0.60	13.30	1.0568	18.0	0.0161	0.0173	0.0620	1.3594	1.4214

[a] Rods 2A, 2C, 4A, and 4C will have matrix compositions of 60% A240 petroleum pitch binder and 40% filler. Rods 2B and 4B will have matrices that are 40% filler, 57% A240 petroleum pitch, and 3% octadecanol additive.

[b] Particle batch number 6154-01-010.

[c] Particle batch number 6542-06-11.

[d] Particle batch number 6641-00-010.

close-to-reference design, BISO coated, 500-μm-diameter, sol-gel ThO_2 kernels during irradiation in the target position of the ORNL HFIR. The coating variables being examined are buffer and OPyC thickness, as well as OPyC density and OPTAF. Each experiment will include particles from seven batches of GGA-coated product and a comparable quantity of ORNL-coated material. A brief description of the GGA particles included in this capsule series was given in an earlier Quarterly Progress Report (Gulf-GA-A12222).

Both HT-12 and HT-13 have completed irradiation. Particles in HT-12 were exposed to a fast neutron exposure of $\sim 4 \times 10^{21}$ n/cm^2 at 1500°C and 2.5×10^{21} at 1100°C. The operating temperatures are estimates made by ORNL. Design temperatures were 1250° and 900°C. Particles in HT-13 were exposed to a fast neutron exposure of $\sim 8 \times 10^{21}$ n/cm^2 in the high-temperature cell and 6×10^{21} n/cm^2 in the low-temperature cell. ORNL has not yet supplied estimated operating temperatures for HT-13; consequently, it will be assumed that HT-13 also operated at 1100°C in the low-temperature cells and 1500°C in the high-temperature cells.

The results of preliminary observations made by ORNL while unloading the particles from HT-12 and -13 are given in Table 9.2. Both experiments indicate that BISO coated particles having OPyC layers with medium-to-high densities (1.80 g/cm^3 to 2.00 g/cm^3) and low-to-medium (≤1.15) OPTAF values show better irradiation behavior than particles with high-density, high-OPTAF OPyC layers.

Postirradiation examination of HT-12 samples is currently under way at GGA, and samples from HT-13 will be included when they arrive from ORNL. Scheduled examinations are radiography, particle density determinations, solid fission product studies, burnup analyses, and metallography. A more detailed discussion of the behavior of the BISO coated ThO_2 particles irradiated in HT-12 and -13, including those that operated at 1500°C in HT-13, will be presented after a complete postirradiation analysis has been performed.

TABLE 9.2

SUMMARY DESCRIPTION OF THE IRRADIATION BEHAVIOR OF GGA FABRICATED, BISO-ThO_2 PARTICLES IN HT-12 AND HT-13

Batch Number	Kernel Diameter (μm)	Buffer		OPyC			Total Coated Particle		Irradiation Behavior (% Survival)			
									HT-12		HT-13	
		Thickness (μm)	Density (g/cm^3)	Thickness (μm)	Density (g/cm^3)	OPTAF	Diameter (μm)	Density (g/cm^3)	1100°C	1500°C	1100°C	1500°C
4252-02-012	503	86	1.08	72	1.84	1.07	829	3.579	100	100	100	12
4252-06-018	511	78	1.10	77	1.82	1.14	826	3.805	98	100	100	0
4252-00-013	408	76	1.26	81	2.00	1.14	721	3.300	100	97	92	0
4252-01-070	495	64	1.11	75	2.02	1.16	783	4.068	100	73	68	0
4252-03-012	501	92	1.00	67	2.00	(a)	820	3.603	100	0	0	0
4252-07-016	489	44	1.03	51	>1.5[a]	1.20	671	4.839	100	75	62	0
4252-08-014	491	40	1.08	120	1.95	1.14	797	3.838	100	40	100	0

[a] Maximum value measurable by Quality Control OPTAF instrument is 1.5

MEASUREMENT OF GAS CONTENT OF IRRADIATED TRISO I $(Th,U)O_2$ PARTICLES

Measurement of the gas content of irradiated fuel particles is continuing to further characterize HTGR fuel. As more gas determination data are accumulated, this investigation will assist in predicting particle failure due to thermochemical reactions and internal stress.

The present experimental work is concerned with the internal gas pressures built up in irradiated and unirradiated TRISO I $(Th,U)O_2$ particles. Although the present reference particle is a TRISO II type, the TRISO I particle can represent a TRISO II whose inner PyC coating has failed. Therefore, the CO and CO_2 gases formed during irradiation are exposed to the SiC coating, which may react with the gases. These reactions would tend to reduce the CO/CO_2 pressures. The purpose of the work conducted during this report period was to measure coated particle gas content and to estimate gas pressures to assist in understanding machanisms controlling gas pressures in irradiated particles.

Materials

A description of both the irradiated and unirradiated TRISO I $(Th,U)O_2$ particles selected from batch 3332-141 is presented in Table 9.3. The particles were irradiated in capsule P13F to a fast neutron exposure of 2.80×10^{21} n/cm^2 (E > 0.18 MeV) and a burnup of 13% FIMA. The average irradiation temperature was 1255°C.

Experimental Procedure

The description of the apparatus and the general analytical procedures used to determine pressures were described in the previous Quarterly Progress Report (Gulf-GA-A12422). The particles were heated to a selected temperature and crushed in order to measure the internal gas released.

TABLE 9.3
DESCRIPTION OF TRISO I $(Th,U)O_2$ PARTICLE BATCH 3332-141

Kernel	
Fabrication process	ORNL sol gel; heat-treated at 1100°C
Diameter	150 to 250 μm range; average 183 μm
Composition	$(Th,U)O_2$ (U, 97.65% enriched)
Th/U ratio	3.0
Density	8.6 g/cm^3
Percent theoretical density	84%
Buffer layer[(a)]	
Coating gas	Acetylene (C_2H_2)
Coating temperature	1100°C
Coating rate	74 μm/min
Thickness	37 μm
Density	1.10 g/cm^3 (estimated)
Percent theoretical density	50%
SiC layer[(a)]	
Coating gas	Methyltrichlorosilane (CH_3SiCl_3)
Coating temperature	1400°C
Coating rate	0.13 μm/min
Thickness	28 μm
Density	3.15 g/cm^3
Percent theoretical density	98%
Outer PyC layer[(a)]	
Coating gas	Methane (CH_4)
Coating temperature	2000°C
Coating rate	1.3 μm/min
Thickness	33 μm
Density	2.00 g/cm^3
Percent theoretical density	90%
BAF	1.00

[(a)] Coating date: February 4, 1966.

Each irradiated and unirradiated particle was microradiographed and each irradiated particle was gamma counted as discussed in an earlier Quarterly Progress Report (Gulf-GA-A10784). From the dimensions of the particle as measured from the radiograph, the maximum and minimum void volumes were determined. The void volume is needed to calculate the pressure inside the particle. Each irradiated sample was gamma counted with a lithium-drifted germanium detector interfaced to a 4069 SDS Sigma II computer analyzer. From these results, the Cs-137/Zr-95 atom ratio of each particle at the end of irradiation was computed.

The theoretical amounts of Kr and Xe produced during irradiation in each particle are determined using Cs-137 as the reference isotope. The assumption that cesium is retained by intact particles is based on relative agreement between the measured and theoretical Cs-137/Zr-95 atom ratios.

The indicated pressure rise in the device upon crushing a particle must be corrected to yield a true value since at constant true pressure the indicated pressure shown by the ionization gauge is a function of gas composition, as shown in Fig. 9.1. The graph indicates that a correction factor (α) needs to be applied to the recorded pressures. The exact composition of the gas released from the particles was not known and, therefore, the correction factor was estimated to be 0.75 which corresponds to the best estimate for a gas composition of about 50.8% CO, 2.9% CO_2, 38.2% Xe, and 8% Kr. All irradiated particle data in Figs. 9.2 through 9.4 were adjusted with this correction factor. No corrections were made for the data from the unirradiated particle experiments.

If the assumption is made that all Kr and Xe atoms are released from the particle during crushing, the CO gas pressure can be estimated by subtracting the theoretical fission gas content from the total measured gas content. All calculations assumed that the gases were ideal.

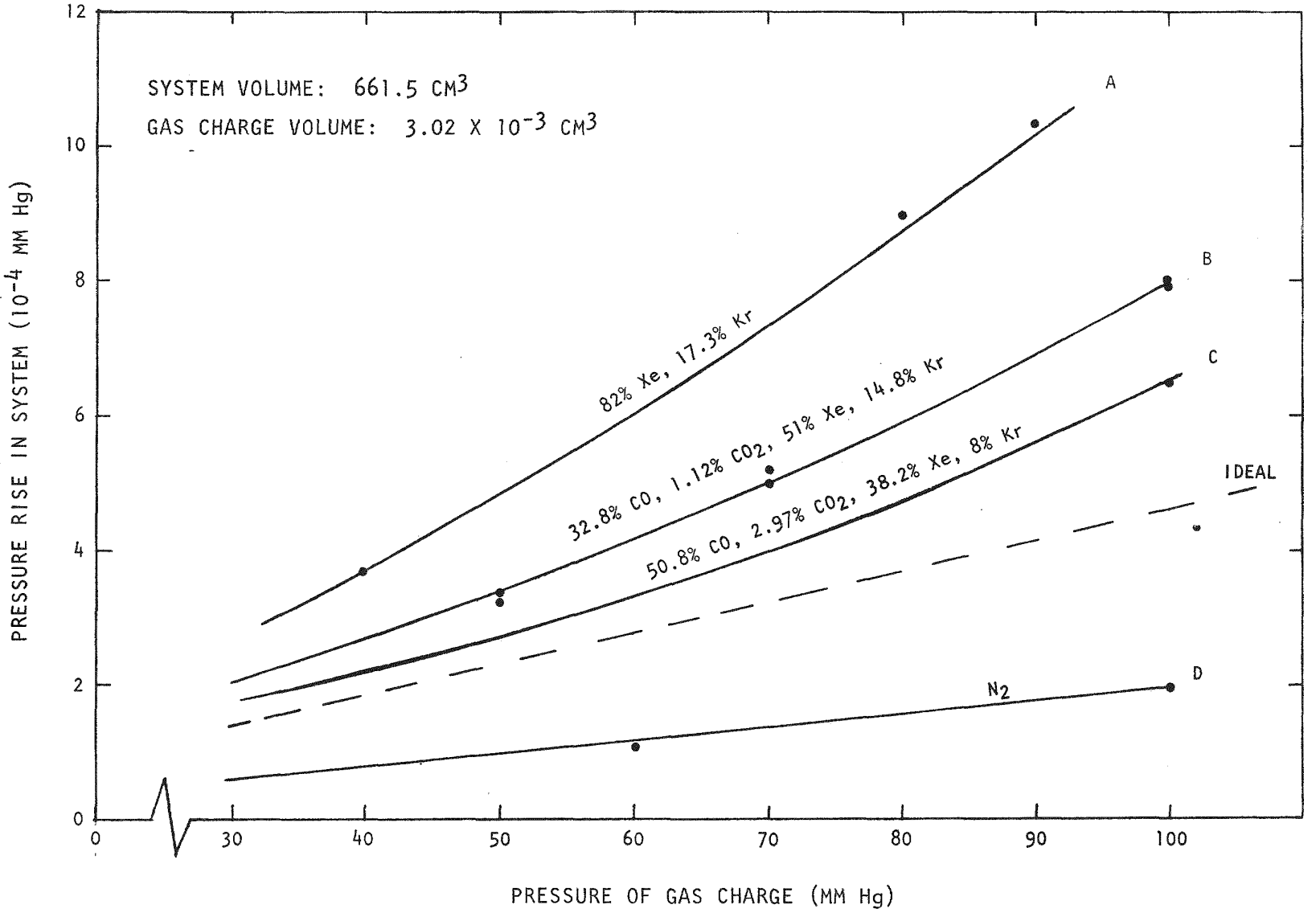

Fig. 9.1. Pressure rise in system vs amount and composition of gas vented to system

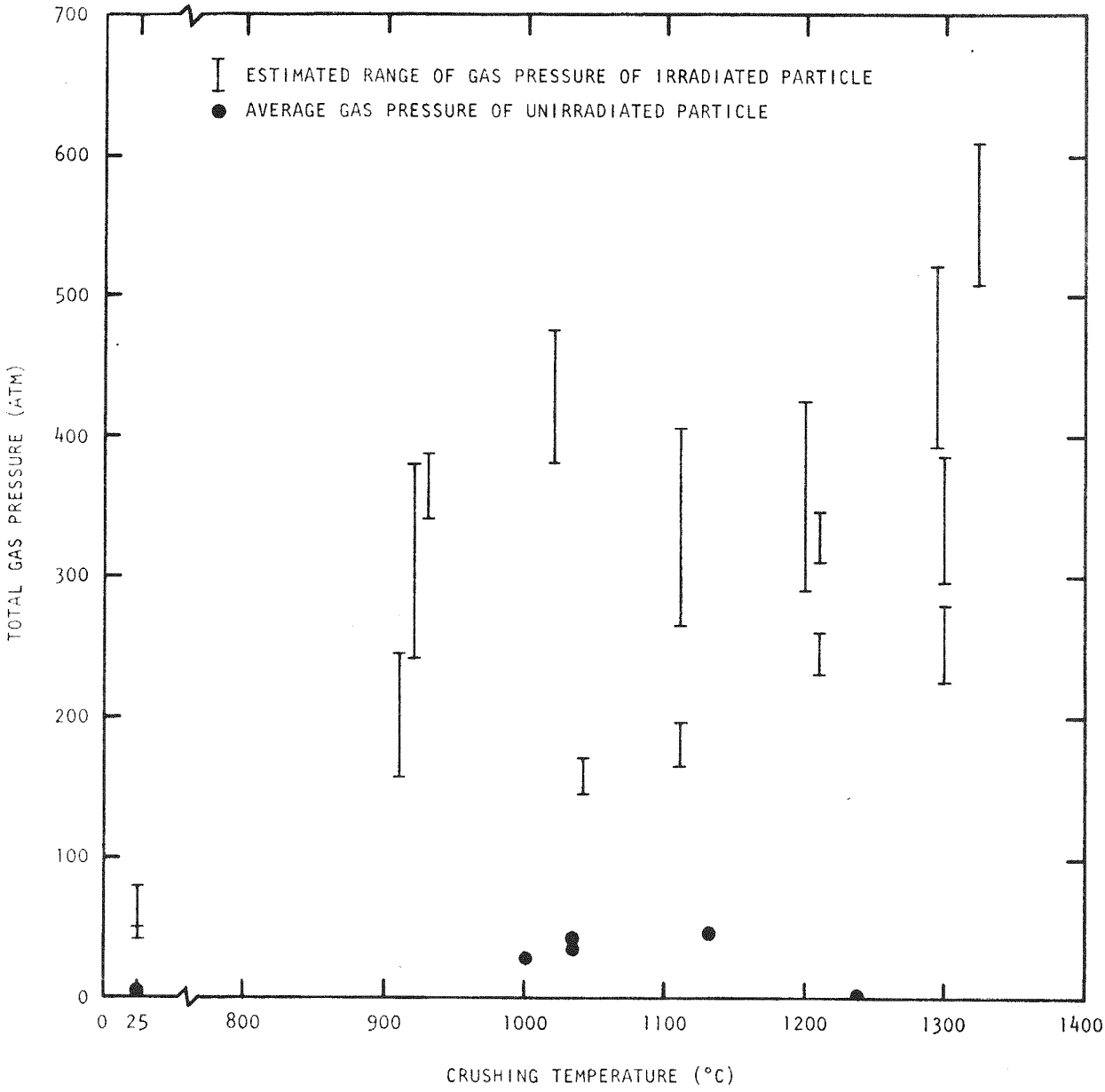

Fig. 9.2. Temperature dependence of total gas pressures of irradiated and unirradiated TRISO I $(Th,U)O_2$ particles

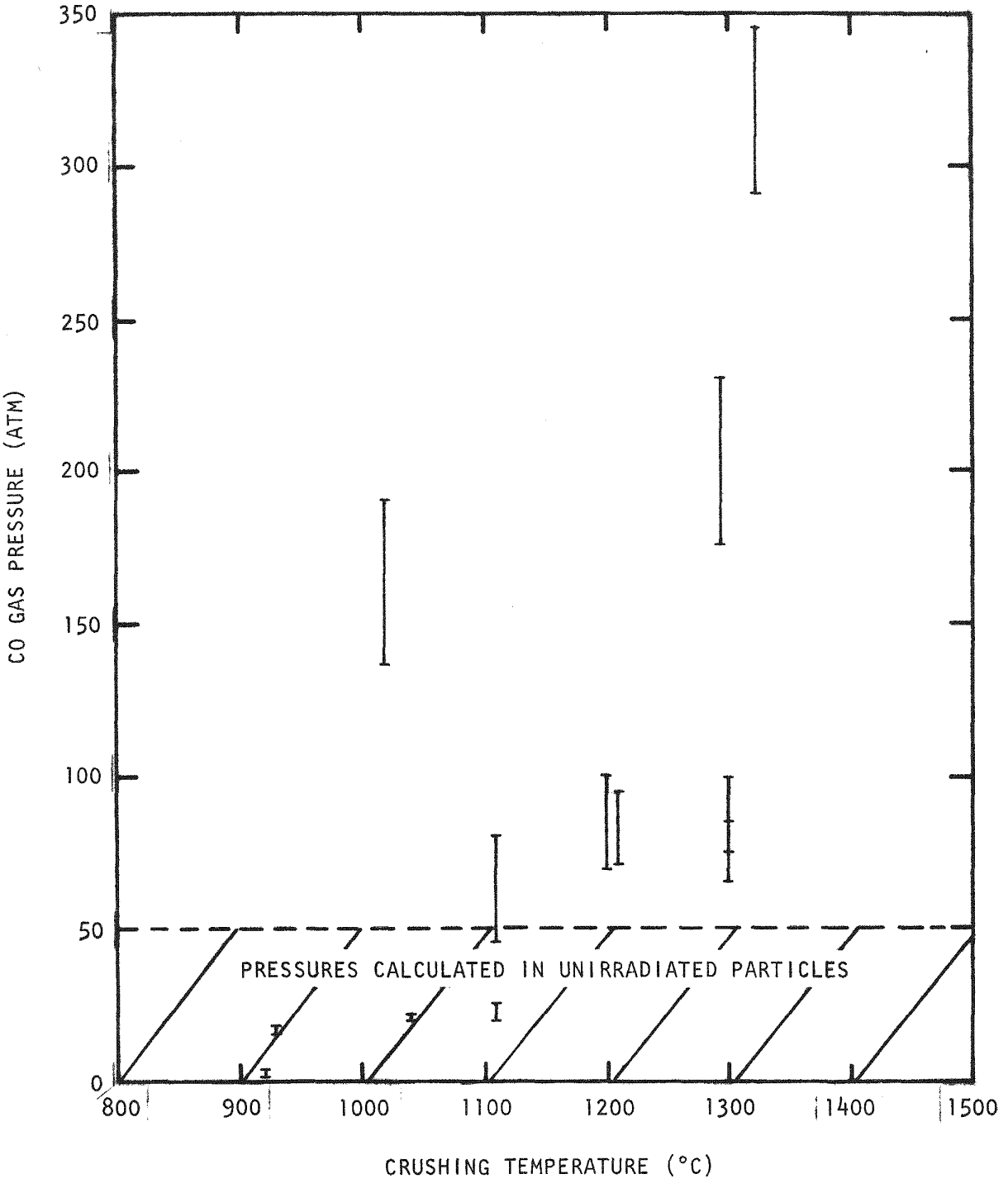

Fig. 9.3. CO gas pressure of irradiated TRISO I $(Th,U)O_2$ particles versus crushing temperature

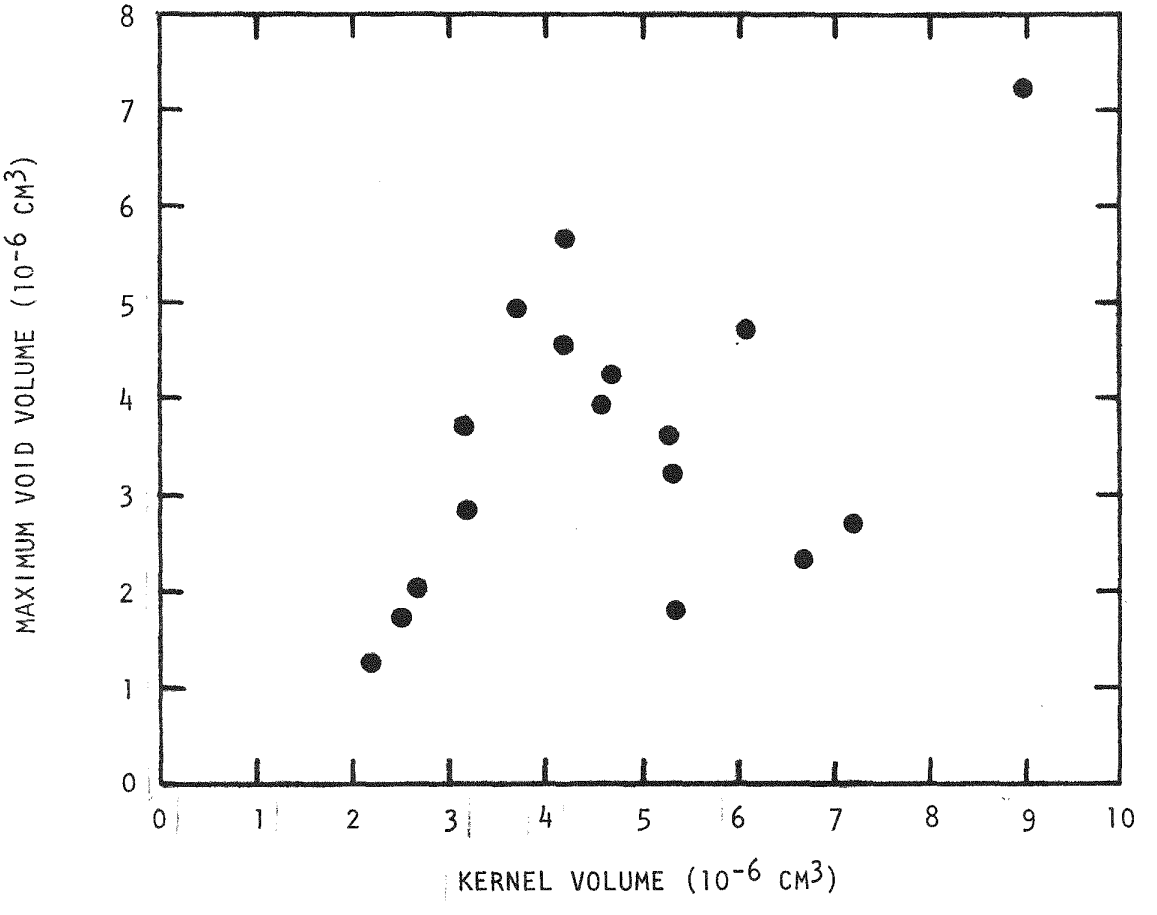

Fig. 9.4. Void volume versus kernel volume in irradiated TRISO I $(Th,U)O_2$ particles

Results and Discussions

Internal gas content was measured in six unirradiated and seventeen irradiated TRISO I $(Th,U)O_2$ particles. The results of the unirradiated particle experiments are presented in Table 9.4, and the irradiated particle gas determinations are given in Table 9.5. Both the kernel and the coatings were crushed as evidenced by microscopic inspection of the crushed particle. After an irradiated particle was initially crushed by lowering the crushing ram, a pressure rise in the testing system was recorded due to the gases being released. The ram was raised and then lowered again to further break up the particle. However, no additional rise in pressure was observed; this can be explained by all free void volume in the kernel and buffer coating in an irradiated particle being interconnected and, therefore, all gas being released upon initial crushing.

The total gas pressure of each irradiated and unirradiated particle as a function of the crushing temperature is plotted in Fig. 9.2. Pressures as high as 600 atm were calculated in the irradiated particles and 50 atm in the unirradiated samples.

The composition of the gas released in the unirradiated particles is unknown. It may be CO/CO_2 gas generated by the reduction of the hyperstoichiometric kernel to $UO_{2.00}$ and/or residual hydrogen content resulting from decomposition of hydrocarbons deposited during the buffer coating process. There is no explanation why one particle had no gas released since it visually appeared to be intact before crushing.

The calculated CO gas pressures versus crushing temperatures for irradiated particles are shown in Fig. 9.3. There is the uncertainty of how much, if any, of the measured total gas content in an irradiated particle was there before irradiation. The hatched area represents the calculated pressures of the unirradiated particles. The CO pressures may be lower by this amount. However, significant CO gas appears to be formed

TABLE 9.4
RESULTS OF GAS CONTENT DETERMINATIONS IN
UNIRRADIATED TRISO I $(Th,U)O_2$ PARTICLES
(Batch 3332-141)

Experiment Number	Crushing Temp (°C)	Kernel Volume (10^{-6} cm^3)	Particle Void Volume (10^{-6} cm^3)		Total Gas Volume at 1 atm, 298°K[(a)] (10^{-4} cm^3)	Calculated Total Gas Pressure at Crushing Temp (atm)	
			Min.	Max.		Min.	Max.
6046-10	25	5.42	5.30	6.54	0.19	3	4
5847-136	1000	3.54	4.37	4.96	0.28	24	27
5847-138	1035	2.18	2.75	2.88	0.23	35	37
5847-142	1035	6.37	4.84	6.32	0.47	33	43
5847-140	1135	4.06	5.27	6.05	0.56	44	50
5847-134	1240	5.50	3.43	4.72	0	0	0

(a) Calculated from measured gas content at pressures $<10^{-3}$ Torr assuming the ideal gas law.

TABLE 9.5
RESULTS OF GAS CONTENT MEASUREMENTS IN TRISO I $(Th,U)O_2$ PARTICLES IRRADIATED IN CAPSULE P13F
(1255°C, 13% FIMA, BATCH 3332-141)

Experiment Number	Crushing Temp (°C)	Kernel Volume (10^{-6} cm^3)	Particle Void Volume (10^{-6} cm^3)		Cs-137/Zr-95 Atom Ratio[a] (Theoretical ratio = 1.85)	Theoretical Kr + Xe Volume at 1 atm, 298°K[b] (10^{-4} cm^3)	Total Gas Volume at 1 atm 298°K[c] (10^{-4} cm^3)	Total Gas Pressure at Crushing Temp (atm)				Theoretical Kr + Xe Gas Pressure at Crushing Temperature (atm)		Estimated CO Pressure at Crushing Temperature[e] (atm)	
								Uncorrected		Corrected[d]					
			Min.	Max.				Min.	Max.	Min.	Max.	Min.	Max.	Min.	Max.
5847-86	25	6.70	3.35	5.02	1.82	2.32	3.46	69	103	52	77	46	69	6	8
5847-90	25	7.24	3.35	5.24	1.89	2.74	3.51	67	105	50	79	52	82	< 0	< 0
5847-124	25	5.35	3.12	4.32	1.93	1.76	2.10	49	67	37	50	51	56	< 0	< 0
5847-100	910	8.99	4.74	7.24	1.75	2.83	3.89	213	326	160	244	156	236	4	< 0
5847-96	920	5.35	1.99	3.20	1.38	1.86	2.54	317	510	238	382	232	374	6	8
5847-108	930	2.23	1.10	1.25	1.62	0.85	1.40	451	513	338	384	297	337	41	47
5847-92	1020	2.52	1.43	1.68	1.88	0.94	2.10	504	634	378	475	242	285	136	190
5847-112	1040	4.19	4.76	5.58	1.68	1.54	2.45	193	226	145	169	121	142	24	27
5847-116	1110	5.21	2.41	3.58	1.60	1.68	2.80	352	538	264	403	217	322	47	81
5847-120	1110	3.71	4.24	4.90	1.94	1.50	2.36	223	258	167	194	142	167	25	30
5847-126	1200	6.12	3.19	4.66	1.32	2.12	3.67	389	568	292	426	222	327	70	99
5847-114	1210	2.71	1.78	2.00	2.07	0.91	1.66	411	463	308	347	226	254	82	93
5847-118	1210	3.16	3.22	3.68	1.57	1.16	2.27	306	350	229	262	157	179	72	83
5847-106	1295	4.58	2.93	3.89	2.46	1.60	3.85	523	693	392	519	217	288	175	231
5847-122	1300	4.19	3.73	4.55	1.41	1.36	2.62	297	370	223	278	157	192	66	86
5847-128	1300	4.71	3.21	4.21	1.74	1.76	3.14	393	516	295	387	220	289	75	98
5847-110	1325	3.16	2.37	2.84	1.64	1.16	3.58	676	812	507	609	219	263	288	346

[a] Because of a relatively short half-life, the Zr-95 content was extremely small; therefore, the more readily measured Cs-137/Ru-106 ratio was used to estimate the more commonly measured Cs-137/Zr-95 ratio.

[b] Calculated by the FISS/PROD program as described in the text.

[c] Calculated from measured gas content at pressures $<10^{-3}$ Torr assuming the ideal gas law.

[d] Correction factor (α) = 0.75.

[e] Corrected total gas pressure minus theoretical Kr + Xe gas pressure.

in some of the particles, especially at the higher temperatures. The pressures produced by the CO gas are much higher than the equilibrium pressure of CO gas in the $SiC/SiO_2/C$ system, which is less than one atmosphere* in this temperature range.

It can be seen that in a small temperature range, the pressures vary appreciably. The order of magnitude differences in void volume and kernel volume in individual particles contributed to the variability in calculated gas pressures. The maximum void volume versus the kernel volume of each particle is shown in Fig. 9.4. The lack of uniform particle size helps to explain why there is a large range of calculated pressures at a given temperature.

This investigation indicated that relatively high internal gas pressures can build up in irradiated TRISO I $(Th,U)O_2$ particles with a Th/U ratio of three at temperatures of irradiation. Internal gas content measurements of both irradiated and unirradiated coated particles are continuing to further characterize the fuel.

---

*Flowers, R. H., and G. W. Horsley, Dragon Project, "The Influence of Oxide Kernels in the Manufacture and Performance of Coated Particle Fuel," unpublished data.

TASK XI
GRAPHITE RESEARCH

INTRODUCTION

Work during the current quarter was divided among three major tasks: (1) design of a graphite capsule for insertion in the ORR, (2) property measurements and irradiation of production-grade near-isotropic and needle-coke graphites, and (3) pyrolytic carbon irradiation studies. The capsule (OG-1) will provide an irradiation vehicle for moderator graphites along with smaller quantities of pyrolytic carbons, silicon carbide, boronated control graphites, and fuel stick matrix materials.

CAPSULE DESIGN AND FABRICATION

A description of the capsule was given in the previous Quarterly Progress Report (Gulf-GA-A12422). The capsule will operate at 600° to 1400°C to fluences of approximately 0.5 to 3.5 x 10^{21} n/cm^2 (E > 0.18 MeV). Capsule irradiation was scheduled to begin in the C-3 position in February. However, some delay was encountered while materials that met the RDT Quality Assurance Standards were located (at ORNL) and ordered. The graphite crucibles have been fabricated and are ready for loading. It is expected irradiation will begin in June 1973.

Thermal analysis has been completed based on gamma heating data from ORNL. All design temperatures were met by the selection of suitable heat transfer gaps. The analysis was based upon nonirradiated graphite properties and the design case was based on a gas-gap thermal conductivity of 40% argon and 60% helium. In addition, thermal analyses of off-design cases (viz, 80%, 100%, and 120% design gamma heating with 100% helium gas and 100% gamma heating with 100% argon gas) were also performed.

GRAPHITE IRRADIATION STUDIES

Several new graphites are under study along with Grade H-327 which is the graphite used for Fort St. Vrain. (See Table 11.1 for description of graphites.) Impurity content, thermal expansivity, and tensile strength data were presented in the previous Quarterly Progress Report (Gulf-GA-A12422) for graphites H-451 and H-453. Additional values of tensile strength and modulus of elasticity have been obtained on specimens from H-451 and H-453. The new data are presented in Tables 11.2 and 11.3, respectively. Impurity content was measured on Grades 2020, 9567, and P_3JHAN (see Table 11.4).

The new tensile data were obtained on specimens 0.25-in. in diameter by 0.90 in. long, whereas the values reported in Gulf-GA-A12422 were measured on specimens 0.50-in. in diameter by 4 in. long. The procedure in both tests is identical except for specimen and specimen holder sizes. The smaller specimens were tested for comparison with data from the larger specimens, which are the current standard specimen size for testing unirradiated material (see Table 11.5). Specimens of the smaller dimensions will be irradiated in capsule OG-1 and will be the only size available for postirradiation testing.

The H-451 strength data show good agreement between small and large samples in the direction parallel to extrusion, but the values of the small specimens were somewhat higher than those for the larger specimens when measurement was made in the direction perpendicular to extrusion. This trend was also noted for graphite H-453. A possible explanation for this behavior may be the existence of flaws in the form of fine cracks lying parallel to the direction of extrusion. These flaws would be included in the large perpendicular samples but not in the smaller ones. A second log of H-451 is being tested to further evaluate this phenomenon. Graphite H-451 is stronger near the diametral edge of the log than near the center, whereas H-453 appears to be more uniform. Such a strength gradient is common in large extruded graphite logs.

TABLE 11.1
DESCRIPTION OF NUCLEAR GRAPHITES

Grade	Source	Coke Type	Binder	Impregnant	Remarks
H-327	Great Lakes Carbon Co. (GLCC)	Needle	Coal-tar pitch	Coal-tar pitch	Graphite used for Fort St. Vrain
9567	AirCo Speer	Needle	Coal-tar pitch	Coal-tar pitch	Recently manufactured for HTGR program
H-451	GLCC	Near-isotropic	Coal-tar pitch	Petroleum pitch	Recently manufactured for HTGR program
H-453	GLCC	Near-isotropic	Coal-tar pitch	Petroleum pitch	Recently manufactured for HTGR program
2020	Stackpole Carbon Co.	Near-isotropic	--	--	Molded
P_3JHAN	Pechiney	Near-isotropic	--	--	Being studied for comparison with U.S. graphites

TABLE 11.2
TENSILE STRENGTH OF GRAPHITES H-451 AND H-453
(Specimen Size: 0.25-in. diameter by 0.90 in. long)

Tensile Strength (psi)											
Mid-Length Center				Mid-Length Edge				End Center			
H-451		H-453		H-451		H-453		H-451		H-453	
∥	⊥	∥	⊥	∥	⊥	∥	⊥	∥	⊥	∥	⊥
1680	1490	1570	1500	2320	2040	1960	1100	1290	2380	2440	1420
1750	1540	1960	1660	2120	1140	1370	1310	1710	2080	2360	1790
1800	1640	1950	1370	2220	1730	1830	1560	1690	1690	2260	1570
1970		2040		2220		2140		1670		2160	
1770		2240		2200		1910		1730		2200	
1870		1750		2240				1550		2240	
1720		1690		2400				1970			
		2240									
Average (One Sigma)											
1794	1556	1955	1510	2245	1637	1842	1323	1659	2050	2276	1593
(90)	(62)	(220)	(205)	(83)	(373)	(257)	(326)	(190)	(281)	(95)	(152)

TABLE 11.5
COMPARISON OF TENSILE DATA FROM SMALL AND LARGE SPECIMENS FOR GRAPHITES H-451 AND H-453

Orientation	H-451		H-453	
	0.50 x 4.0 in.	0.25 x 0.90 in.	0.50 x 4.0 in.	0.25 x 0.90 in.
	Mid-Length Center			
∥	1884 ± 45	1794 ± 90	1973 ± 87	1955 ± 220
⊥	1078 ± 157	1556 ± 62	1170 ± 185	1510 ± 205
	Mid-Length Edge			
∥	2173 ± 142	2245 ± 83	1844 ± 126	1842 ± 257
⊥	1260 ± 46	1637 ± 373	1363 ± 277	1323 ± 326
	End Center			
∥	1892 ± 126	1659 ± 190	1919 ± 217	2276 ± 95
⊥	1367 ± 139	2050 ± 281	1170 ± 185	1593 ± 152

Graphites 9567 and P_3JHAN, which were purified during manufacture, meet purity specifications for HTGR design. Graphite 2020 has excessive silicon and boron concentrations; however, this particular sample was not originally intended for nuclear application. It is believed this grade can be produced to meet HTGR specifications.

Tensile strength and modulus of elasticity data are being obtained on graphites 9567, P_3JHAN, and 2020.

PYROLYTIC CARBON IRRADIATION STUDIES

Preparation of specimens for irradiation in capsule OG-1 has been completed. The specimens include unrestrained LTI and silicon-doped carbons previously irradiated in the BNWL Graphite Capsules (GEH series), a new series of restrained and unrestrained LTI carbons, and a series of LTI and silicon-doped carbons that were restrained in previous irradiations but which will be unrestrained in the OG-1 irradiation.

A series of restrained and unrestrained LTI carbons have also been prepared for irradiation in piggy-back positions in capsule P13Q.

A significant observation on the irradiation behavior of LTI carbons was made in this period. Namely, it was observed that restraint during irradiation alters the preferred orientation of the carbon and that due to this effect carbons which previously had been restrained change dimensions at a much faster rate than carbons which had previously not been restrained. Hints of an increase in preferred orientation due to restraint have been known for some time due to an increase in the optical activity of carbons on coated particles (Ref. 11.1), but the effect is obscured by an increase in the preferred orientation of unrestrained carbons under some irradiation conditions.

A series of carbons restrained on different graphite substrates to produce different degrees of restraint were irradiated along with unrestrained carbons in capsule GEH-13-422. The degree of preferred orientation was measured after irradiation and was found to increase with increasing degree of restraint, i.e., with increasing creep strain.

With the assistance of ORNL personnel, three LTI carbon specimens irradiated restrained and unrestrained in the HRB-1 capsule, were reirradiated unrestrained in the HT-12 capsule. The results are given in Table 11.6. In the second irradiation, the previously restrained specimens changed dimensions at a much faster rate than the previously unrestrained specimens.

The effect of restraint on the dimensional changes obviously must be taken into account in coated particle model calculations. It is planned to investigate this effect in future irradiations, and current data are being analyzed for use in model calculations.

REFERENCE

1. Hewette, D. M., "High-Temperature Fast-Neutron Irradiation of Pyrolytic-Carbon-Coated ThO_2 Microspheres," Carbon 7, 373 (1969).

TABLE 11.6
COMPARISON OF IRRADIATION DATA FOR PREVIOUSLY UNRESTRAINED AND RESTRAINED SPECIMENS

CAPSULE HRB-5-1
Temperature: ∿700°C; Fast Fluence: ∿5 x 10^{21} n/cm^2

Initial Density (g/cm^3)	Dimensional Change ∥ to Deposition Plane	Dimensional Change ⊥ to Deposition Plane	Creep Strain in Restrained Specimen
1.58	-0.097	-0.026	0.009
1.755	-0.074	0.003	0.014
1.509	-0.111	-0.032	0.029

CAPSULE HT-12
Temperature: ∿900°C; Fast Fluence: ∿1.75 x 10^{21} n/cm^2

	Previously Unrestrained Specimen		Previously Restrained Specimen	
Initial Density (g/cm^3)	Dimensional Change ∥ to Deposition Plane	Dimensional Change ⊥ to Deposition Plane	Dimensional Change ∥ to Deposition Plane	Dimensional Change ⊥ to Deposition Plane
1.58	-0.001	0.005	-0.032	0.030
1.755	-0.006	0.015	-0.022	0.025
1.509	-0.006	0.017	-0.044	0.046

APPENDIX

PROJECT REPORTS PUBLISHED DURING THE QUARTER

There were no topical reports published during this period.